THE JOURNAL OF BIOLOGICAL CHEMISTRY VOL. 291, NO. 23, pp. 12254–12270, June 3, 2016

Modulation of P2X3 and P2X2/3 Receptors by Monoclonal Antibodies*

Received for publication, February 16, 2016, and in revised form, April 18, 2016 Published, JBC Papers in Press, April 20, 2016, DOI 10.1074/jbc.M116.722330

Anatoly Shcherbatko[‡1,2], Davide Foletti[‡1], Kris Poulsen[‡1], Pavel Strop[‡], Guoyun Zhu[‡], Adela Hasa-Moreno[‡], Jody Melton Witt[‡], Carole Loo[‡], Stellanie Krimm[‡], Ariel Pios[‡], Jessica Yu[‡], Colleen Brown[‡], John K. Lee[§], Robert Stroud[¶], Arvind Rajpal[‡], and David Shelton[‡]

From the [‡]Rinat Laboratories, Pfizer Inc., South San Francisco, California 94080, the [§]Department of Biochemistry, Molecular Biology, and Biophysics, University of Minnesota, Minneapolis, Minnesota 55455, and the [¶]Department of Biochemistry and Biophysics, University of California, San Francisco, California 94158

Purinergic homomeric P2X3 and heteromeric P2X2/3 receptors are ligand-gated cation channels activated by ATP. Both receptors are predominantly expressed in nociceptive sensory neurons, and an increase in extracellular ATP concentration under pathological conditions, such as tissue damage or visceral distension, induces channel opening, membrane depolarization, and initiation of pain signaling. Hence, these receptors are considered important therapeutic targets for pain management, and development of selective antagonists is currently progressing. To advance the search for novel analgesics, we have generated a panel of monoclonal antibodies directed against human P2X3 (hP2X3). We have found that these antibodies produce distinct functional effects, depending on the homomeric or heteromeric composition of the target, its kinetic state, and the duration of antibody exposure. The most potent antibody, 12D4, showed an estimated IC_{50} of 16 nM on hP2X3 after short term exposure (up to 18 min), binding to the inactivated state of the channel to inhibit activity. By contrast, with the same short term application, 12D4 potentiated the slow inactivating current mediated by the heteromeric hP2X2/3 channel. Extending the duration of exposure to ~20 h resulted in a profound inhibition of both homomeric hP2X3 and heteromeric hP2X2/3 receptors, an effect mediated by efficient antibody-induced internalization of the channel from the plasma membrane. The therapeutic potential of mAb12D4 was assessed in the formalin, complete Freund's adjuvant, and visceral pain models. The efficacy of 12D4 in the visceral hypersensitivity model indicates that antibodies against P2X3 may have therapeutic potential in visceral pain indications.

Extracellular ATP and its metabolites bind and activate their cognate cell membrane receptors, namely the P1 and P2 purinergic receptors. In mammalian cells, seven different subunits (P2X1–7) have been found to compose the family of ATP-gated cation channel receptor subtypes, which play important roles in diverse physiological and pathological processes (1, 2). Each P2X receptor is an oligomer assembled as either a homo- or a heterotrimer (3). Individual subunits surround a central cation pore, and each is composed of two transmembrane spanning segments (TM1 and TM2) connected by a large extracellular domain (~300 amino acid residues) containing 10 conserved cysteine residues (4). Two reported crystal structures of the zebrafish P2X4 ion channel, one in its apo-state (5) and the other in complex with ATP (6), fully elucidate the trimeric structure of the channel and the topology of the individual subunits.

Functional P2X receptors are widely expressed in neuronal and non-neuronal cells and tissues of almost all main organs in the body (7). ATP-gated receptors are implicated in both transient signaling, such as intercellular communications, and long lasting signaling, such as cell growth, differentiation, and proliferation. P2X-mediated neurotransmission and neuromodulation are well established in different regions of the peripheral and central nervous system. ATP signaling is involved in neuron to neuron, neuron to glia, and neuron to muscle cell interactions (8). There is a growing body of evidence suggesting a crucial role of P2X receptors in the pathophysiology of visceral pain (9), neuropathic and inflammatory pain (10), bone cancer pain (11), and head and neck cancer pain (12). P2X receptors are increasingly considered as therapeutic targets for the management of pain (13, 14). In particular, the P2X3 and P2X2/3 subtypes of ATP-gated ion channels are increasingly recognized as playing an important role in nociception due to their predominant expression in sensory neurons (15–17).

In the past decade, efforts to develop purinergic drugs mostly involved high throughput screening of small molecule compound libraries (18, 19). This approach has led to recent development of orally bioavailable selective antagonists of P2X receptors (20–24). AF-219, a small molecule antagonist of human P2X3 receptors developed by Afferent Pharmaceuticals has entered clinical studies in osteoarthritic joint pain, bladder pain syndrome/interstitial cystitis, and asthma patients (24). Furthermore, this molecule has been evaluated in patients with refractory chronic cough in a double-blind, placebo-controlled trial and has shown substantial reductions in daytime cough frequency and also statistically significant improvements in patient-reported outcomes (25).

We sought to explore the feasibility of targeting P2X3 with antibodies that, due to their remarkable specificity toward their targets and their favorable pharmacokinetics properties (26), are increasingly utilized as therapeutics for the treatment of

* The authors declare that they have no conflicts of interest with the contents of this article.

[1] These authors contributed equally to this work.

[2] To whom correspondence should be addressed: Rinat Laboratories, Pfizer Inc., 230 E. Grand Ave., South San Francisco, CA 94080. Tel.: 650-615-7316; E-mail: anatoly.shcherbatko@pfizer.com.

multiple diseases. Although a function modifying monoclonal antibody against the human P2X7 receptor was successfully generated several years ago by cell immunization (27), obtaining modulatory antibodies against multispanning membrane proteins like ion channels is regarded as particularly challenging. Therefore, to increase the chance of obtaining antibodies that recognize the native P2X3 receptor, we utilized recombinantly expressed P2X3 purified in its native conformation in the presence of detergents as immunogen to raise antibodies by standard hybridoma technology. Using this approach, we generated, to our knowledge for the first time, monoclonal antibodies that potently impact the functional activity of P2X3 and P2X2/3 receptors. We have extensively analyzed the mechanism of action of the mAbs and have tested their therapeutic activity *in vivo*.

Experimental Procedures

Protein Expression and Purification—hP2X3[3] with an N-terminal FLAG tag was cloned into the pACMV-tetO vector with expression under control of a tetracycline-inducible promoter. Stably transfected HEK293S GnTI cells (28) were generated by selecting for successful integration of the *neo* gene using the selection agent Geneticin. Stably transfected hP2X3 HEK293S GnTI cells were grown in DMEM (without calcium salts) in a 10-liter wave bag, and hP2X3 expression was induced by the addition of 5 mg/liter sodium pantothenate and 2 mg/liter doxycycline. Cells were harvested by centrifugation ~30 h after induction. Cells resuspended in lysis buffer (50 mM phosphate, pH 7.4, 300 mM NaCl, PMSF, Roche protease inhibitors, 10 mM EDTA) were lysed using a microfluidizer. Lysed cells were first spun at low speed (5,000 × *g*) to remove cellular debris, followed by a high speed centrifugation step (45,000 × *g*) to isolate membranes. Membranes were homogenized and solubilized for 1 h in 50 mM phosphate, pH 7.4, or Tris, pH 7.0, 150 mM NaCl, 10% glycerol, 1% β-dodecylmaltoside, 0.01% cholesterol hemisuccinate, PMSF, and Roche protease inhibitors. Insoluble material was removed by an additional high speed spin (200,000 × *g*). hP2X3 protein was allowed to bind to FLAG resin (Sigma) for 3 h at 4 °C; washed with 50 mM Tris, pH 7.0, 150 mM NaCl, 10% glycerol, 0.1% β-dodecylmaltoside, 0.01% cholesterol hemisuccinate (wash buffer); and eluted with 3× FLAG peptide (Sigma). As a final step, hP2X3 was further purified by size exclusion chromatography using a 10/300 Superdex200 (GE Healthcare) column in wash buffer. Fractions corresponding to the hP2X3 trimer (~150 kDa) were collected and adjusted to a final concentration of 1 mg/ml.

Antibody Generation—Mouse monoclonal antibodies were generated by standard hybridoma technology using BALB/c mice immunized with the purified recombinant hP2X3 described above. Gerbu Adjuvant MM#3001 was used following the manufacturer's instructions (Gerbu Biotechnik GmbH, Gaiberg, Germany), and the myeloma cell line P3 × 63Ag8.653 was used as a fusion partner for splenocytes. BALB/c mice were immunized intraperitoneally and subcutaneously on days 0, 6, 14, 22, 28, and 42. On day 49, the mice were given a prefusion boost without the Gerbu adjuvant, and then the splenocytes were fused 4 days later on day 53.

Electrophysiology—P2X-mediated currents were recorded using either an automated patch clamp system QPatch HT, (Sophion, Biolin Scientific, Denmark) or a conventional patch clamp set-up employing an EPC 10 patch clamp amplifier (HEKA Electronik Dr. Schulze GmbH, Lambrecht/Pfalz, Germany).

QPatch Electrophysiology—Both single-hole and 10-hole QPlates with an integrated 250-μl waste container (QPlate 48L or 48X) were used, enabling washes and application of multiple concentrations/compounds per well. Compounds were added to the cells with the eight pipettes via the QPlate integrated glass microfluidic pathways. Usually, 5 μl of ligand was added for 3 s, followed by washout (six times with 5 μl of saline). Test compounds were typically preincubated for 345 s before the addition of agonist. The ligand induced currents were acquired at 5 kHz for 5 s. During whole-cell recording, the membrane potential was held at −90 mV. The extracellular recording solution contained 137 mM NaCl, 4 mM KCl, 10 mM HEPES, 1.8 mM $CaCl_2$, 1 mM $MgCl_2$, 10 mM glucose, 10 mM sucrose, adjusted to pH 7.4. The intracellular solution contained 130 mM CsF, 10 mM NaCl, 5 mM EGTA, 10 mM HEPES, 4 mM Na_2ATP, and 0.1 mM Tris-GTP, adjusted to pH 7.2. All QPatch data were analyzed using Sophion's QPatch Assay software. Results are presented as mean ± S.E. Statistical analysis was done in Excel with a two-sample *t* test assuming equal variances.

Manual Patch Clamp Electrophysiology—Manual whole-cell patch clamp recordings were obtained from both stably transfected cells and primary neurons. Coverslips carrying cells were placed in a recording chamber and were constantly perfused at a rate of 0.5 ml/min with extracellular solution containing 140 mM NaCl, 5 mM KCl, 2 mM $CaCl_2$, 2 mM $MgCl_2$, 10 mM HEPES, and 10 mM glucose (pH 7.4, 320 mosmol). Patch electrodes were pulled from borosilicate glass and fire-polished to 3–10-megaohm tip resistance. The internal pipette solution (ATP-regenerating solution, pH 7.3, 300 mosmol) consisted of 100 mM KCl, 2 mM $MgCl_2$, 5 mM MgATP, 0.1 mM GTP, 15.5 mM phosphocreatine, 50 units/ml creatine phosphokinase, 10 mM BAPTA tetrapotassium salt, and 10 mM HEPES. All recordings were made at room temperature (22–24 °C) using an EPC 10 patch clamp amplifier (HEKA Electronik Dr. Schulze GmbH). Cells were voltage-clamped at −90 mV, and control test responses were routinely recorded for a minimum of 10 min to ensure that the amplitude and kinetics of the response were stable. Data acquisition and analysis were performed with Pulse-PulseFit (HEKA Electronik Dr. Schulze GmbH) and IgorPro (WaveMetrics, Portland, OR). Agonists were applied to individual cells using a laboratory-built piezoelectrically driven rapid application system.

All reagents were purchased from Sigma unless otherwise noted. All data are expressed as means ± S.E.

Cell Culture—The human glial cell line 1321N1 stably expressing recombinant human or rat P2X3 receptors (Pfizer GR&D, Primary Pharmacology Group, Sandwich, UK) were grown in DMEM (catalog no. 10-01-CM, Mediatech, Manassas,

[3] The abbreviations used are: hP2X3 and hP2X2, human P2X3 and P2X2, respectively; DRG, dorsal root ganglion; αβ-meATP, αβ-methylene ATP; TNBS, 2,4,6-trinitrobenzene sulfonic acid; CFA, complete Freund's adjuvant; Ab, antibody.

VA), 10% FBS (JR Scientific, Inc., Woodland, CA), 500 μg/ml G418 sulfate (Mediatech) in 75-cm^2 Falcon culture flasks in an incubator at 37 °C and 6% CO_2 with saturating humidity. For recordings, the cells were dissociated with enzymatic detachment solution Detachin (Genlantis, San Diego, CA) and resuspended in serum-free medium supplemented with 25 mM HEPES and 1% penicillin/streptomycin (Mediatech).

HEK293 cells transiently expressing human P2X2/3 or human P2X4 receptors (EZCells^{TM} TT) were purchased from ChanTest (ChanTest Corp., Cleveland OH). Cryopreserved cells were thawed rapidly and transferred to 75-cm^2 Falcon culture flasks containing growth medium, consisting of DMEM (catalog no. 10-01-CM, Mediatech), 10% FBS (JR Scientific), 1× penicillin/streptomycin (Mediatech). The cells were kept in an incubator at 37 °C and 6% CO_2 with saturating humidity and used for electrophysiological recordings after 2–3 days of culturing.

DRG Primary Cultures—Lumbar DRG (L1–L5) were quickly removed following decapitation of CO_2 anesthetized adult rats. After isolation, ganglia were desheathed and then enzymatically digested in a two-step procedure: 20-min incubation with collagenase A (1 mg/ml; Roche Diagnostics) in Hanks' balanced salt solution at 37 °C (catalog no. 14025, Gibco) and 15-min incubation with collagenase D (1 mg/ml; Roche Diagnostics) and papain (30 units/ml; Worthington) in Hanks' balanced salt solution at 37 °C with gentle agitation on an orbital shaker. Pooled ganglia were transferred to DRG culturing medium containing DMEM/F-12 (Mediatech), 10% FBS (JR Scientific), 1× penicillin/streptomycin (Mediatech) and were gently triturated with the use of Pasteur pipettes, fire-polished to progressively smaller openings. Dissociated neurons were plated on precoated coverslips (poly-D-lysine/laminin; Corning), flooded with DRG medium, and incubated at 29 °C in a humidified 5.5% CO_2 incubator. The cells were used for electrophysiological recordings within 1–2 days *in vitro*.

Calcium Flux Assay—P2X3/1321N1-expressing cells were seeded at 30,000 cells/well in black wall, clear bottom 96-well plates coated with poly-D-lysine (Costar, Fisher) and grown overnight in a 37 °C, 5% CO_2 incubator. The mAbs were diluted in Calcium3 dye at 2× concentration, (Molecular Devices, Sunnyvale, CA) and then added to the cells for a final antibody concentration of 1 μM and a final concentration of Calcium3 dye of 1×. The mAbs were incubated with the cells and Calcium3 dye for 30 min at 37 °C, followed by 15 min at room temperature. Calcium flux was stimulated by the addition of 10 μM $\alpha\beta$-meATP (Tocris Bioscience, Bristol, UK) and recorded using a FlexStation II 384 platform (Molecular Devices) with the following settings: excitation wavelength = 485 nm, emission wavelength = 538 nm, cut-off = 515 nm, and a 100-s run time measured with 2-s intervals.

FACS—Cells were harvested using Free Cell Dissociation Solution, Hanks-based (Chemicon, EMD Millipore, Temecula, CA), spun down at 1,000 rpm for 5 min at 4 °C, and washed once with ice-cold Dulbecco's PBS (Mediatech). The cells were resuspended in ice-cold FACS staining buffer containing Dulbecco's PBS without Ca^{2+} and Mg^{2+} (Mediatech), pH 7.4, 1% BSA (Sigma-Aldrich), 10 μg/ml goat IgG (Jackson Immunolabs, Westgrove, PA), and the cell density was adjusted to 1 × 10^7 cells/ml. 100 μl of cell suspension was added to 5-ml polystyrene round bottom tubes (Falcon, Fisher). The primary antibodies were added at 10 μg/ml, and incubation proceeded on ice for 1 h with occasional gentle mixing of the cell suspension. The samples were washed twice with 4 ml of ice-cold Dulbecco's PBS, and 2 μg/ml Alexa 488 goat anti-mouse IgG (H+L) (Life Technologies, Inc.) diluted in FACS staining buffer was added. After incubation at 4 °C for 45 min in the dark, the cells were rinsed as described above. Cells were kept at 4 °C throughout the experiment, and buffers without Ca^{2+}/Mg^{2+} were used to minimize cell clumping. Finally, the cell pellet was resuspended in ice-cold Dulbecco's PBS, and data were acquired on a FACSARIA sorter (BD Biosciences) and analyzed using FlowJo (FlowJo, Ashland, OR).

Immunocytochemistry on Live Cells—hP2X3/1321N1 cells were grown overnight in a 37 °C, 5% CO_2 incubator on poly-D-lysine-coated coverslips (BD Biosciences) in a 12-well plate with DMEM (Mediatech) supplemented with 10% fetal bovine serum (Hyclone, GE Healthcare). Before immunocytochemistry, the medium was aspirated, and cells were washed three times with ice-cold PBS (Mediatech). All of the steps from this point on were done on ice and with ice-cold reagents to minimize channel internalization by endocytosis. Primary antibodies, directly conjugated to Alexa 488 (Alexa Fluor 488 protein labeling kit, A-10235, Thermo Fisher) were added at 10 μg/ml in staining buffer (PBS, 0.5% BSA, 5% goat serum (Life Technologies). Incubation proceeded for 40 min; the cells were rinsed as above and then fixed with 4% formaldehyde (Polysciences, Warrington, PA) for 10 min. After a final rinse, the coverslips were mounted on glass slides with mounting medium ProLong Gold anti-Fade + DAPI as nuclear stain (Invitrogen). For the quenching experiment, the cells were incubated with a rabbit polyclonal anti-Alexa 488 (A-11094, Thermo Fisher, Rockford, IL) at 20 μg/ml for 30–45 min after the fixation step. Microscopy was carried out on a Leica laser-scanning confocal microscope at room temperature (Leica, Buffalo Grove, IL), and images from *z*-stacks with 0.5-μm optical sections were collected using a ×63, 1.4 numerical aperture objective lens. Representative images are shown either as individual *z*-sections or as maximum projections from an entire *z*-stack as generated by the Leica LAS AF software.

Immunocytochemistry on Fixed and Permeabilized Cells—hP2X3/1321N1 cells were grown on poly-D-lysine coverslips as described above. Before immunocytochemistry, the medium was aspirated, and cells were fixed with 4% formaldehyde for 10 min at room temperature. Subsequently, cells were washed three times with PBS and then permeabilized with 0.3% Triton X-100 (Sigma-Aldrich) for 2 min at room temperature. After washing as above, the cells were blocked for 1 h at room temperature in blocking buffer (PBS, 0.5% BSA, 5% normal goat serum (Life Technologies). Primary antibodies were added and incubated for 1 h at room temperature and included anti-P2X3 antibodies directly conjugated to Alexa 488 or Alexa 647 (Alexa Fluor 647 protein labeling kit, A-20173, Thermo Fisher) at 5 μg/ml and rabbit polyclonal antibodies to detect specific intracellular organelles according to the recommendations of the manufacturer. The following antibodies were used: anti-giantin to detect the Golgi compartment (Abcam, Cambridge, MA), anti-EEA1 to detect early endosomes (Abcam), and anti-ca-

thepsin D to detect lysosomes (Calbiochem). The cells were washed as above, and the secondary antibody Cy3-goat anti-rabbit IgG (H+L) (1:400) (Jackson Immunolabs) was added and incubated for 1 h at room temperature. The cells were washed and mounted on slides as described above. For overnight mAb incubation experiments, the antibodies were incubated with cells at 1 μM. Microscopy was carried out as described above.

In Vivo Testing—All experiments were performed under protocols approved by an institutional animal care and use committee in an AAALAC (Association for Assessment and Accreditation of Laboratory Animal Care)-approved facility. All testing was done by experimenters blind to both treatment and group assignment of individual animals.

2,4,6-Trinitrobenzene Sulfonic Acid (TNBS)-induced Colitis—After overnight fasting, rats were anesthetized with ketamine (80 mg/ml)/xylazine (12 mg/ml) (1 ml/kg). An abdominal laparotomy was performed, and a TNBS solution (50 mg at 1.5 ml/kg, TNBS treatment group) or vehicle (sham group) was injected into the proximal colon (1 cm distal from cecum). The fourth day following surgery, the TNBS treatment group was subdivided into two groups, one receiving 12D4 (30 mg/kg i.v.) and the other receiving control IgG (30 mg/kg i.v.). On the seventh day following surgery, after a second overnight fast, TNBS-treated rats were tested for visceral pain threshold with balloon distension. A 5-cm latex balloon attached to a catheter was inserted into the distal colon with the base of the balloon 5 cm from the anus. The catheter was fixed to the tail with tape to prevent balloon movement. After a 30-min acclimation period, the balloon was inflated sequentially from 5 mm Hg to 80 mm Hg in 30-s intervals. Balloon distension was halted at the threshold pressure required to elicit a stereotypical rodent visceral pain posture known as the alpha position, repeated waves of contraction of oblique musculature with inward turning of the hind paw (29), and this was recorded as the visceral pain threshold. Animals were euthanized after the balloon distension test.

0.5% Formalin Test—Three days before testing, female rats received either PBS (vehicle) or 12D4 (30 mg/kg subcutaneously). Rats were routinely handled for 2 days before testing. On the day of testing, rats were habituated to clear, plexiglass arenas for at least 30 min. 50 μl of 0.5% formalin was injected into the plantar surface of the left hind paw. Painlike behavior (persistent flinching) of the injected paw was manually recorded (number of flinches per 5-min interval) for 60 min.

Complete Freund's Adjuvant (CFA) Model of Inflammatory Pain—Three days before CFA injection, animals were tested for baseline withdrawal latency to a noxious thermal stimulus and then received treatment (control IgG or 12D4 (30 mg/kg subcutaneously)). Baseline and post-treatment withdrawal latencies to a noxious thermal stimulus were measured using the radiant heat test (30) using a plantar test apparatus (IITC (Woodland Hills, CA), model 390). The stimulus intensity was set such that the pre-injury withdrawal latencies were 15–18 s. The cut-off time was set at 30 s. Rats were placed on a glass platform warmed to 30 ± 2 °C and allowed to habituate to the testing chambers for a minimum of 15 min before each test session. The thermal stimulus was applied to the plantar surface of the paw, and three readings per rat per paw were taken at each test session. Thermal thresholds are defined as the latency in seconds to the first pain behavior, which includes nocifensive paw withdrawal, flinching, and biting and/or licking of the stimulated paw. Three readings for each paw per animal were averaged at each individual time point, the mean and S.E. were determined for the injured and normal paws for each treatment group. Withdrawal latencies to noxious thermal stimulus were tested before treatment, before CFA injection, and 48 h after CFA injection.

Results

Antibody Generation and Initial Screening—The full-length human P2X3 molecule was expressed recombinantly in mammalian cells (HEK293) and purified by affinity and size exclusion chromatography. The purification was performed in the presence of a mild detergent (β-dodecylmaltoside) to help preserve the native oligomeric state of the channel. The same detergent was previously utilized to solubilize and purify the P2X4 channel for crystallographic studies (31). This antigen was then used to immunize mice and obtain mAbs by standard hybridoma technology. Initial screening of mAbs was conducted by FACS on a cell line engineered to stably and functionally express human P2X3 on the background of the astrocytoma cell line 1321N1, hP2X3/1321N1 (32). FACS on live cells comparing the signal obtained on P2X3/1321N1 with the signal obtained on the parental cells (1321N1) identified a panel of antibodies able to specifically bind P2X3 in a native plasma membrane environment (data not shown). The ability of these mAbs to specifically bind the native conformation of the channel was confirmed by immunocytochemistry, as exemplified for mAb 12D4. Whereas 12D4 specifically binds the channel and stains the plasma membrane of hP2X3/1321N1 cells when incubated with live cells (Fig. 1, *A–C*), the antibody detects intracellular P2X3 after cell fixation and permeabilization in a specific distribution pattern. P2X3 appears to be localized in a set of intracellular organelles with a distinct punctate pattern that overlaps only minimally with the Golgi complex (Fig. 1*D*) and partially with early endosomes (Fig. 1*E*).

We then used a Ca^{2+} flux assay with the hP2X3/1321N1 cell line to test the ability of these mAbs to modify the activity of the channel, making use of its ATP-activated inward conductance of calcium ions. Cells seeded in 96-well plates were incubated with antibodies at 1 μM, and a calcium sensitive fluorescent dye for 45 min before calcium flux was stimulated with the addition of 10 μM $\alpha\beta$-meATP. Several antibodies decreased the Ca^{2+} influx to various extents (data not shown) and were therefore taken into a more extensive electrophysiological characterization employing the whole-cell voltage clamp technique.

Anti-hP2X3 mAbs "Acutely" Inhibit the Activity of Recombinant Homomeric hP2X3 Receptors—hP2X3/1321 cells were used to assess antibody inhibition of 3 μM $\alpha\beta$-meATP-evoked inward currents (Fig. 2). In whole-cell electrophysiological recordings performed on an automated patch clamp system (QPatch), we found a variable degree of hP2X3 receptor function inhibition by the antibodies tested with the short term (up to 18 min) agonist application protocol (Fig. 2*A*). Among the 11 mAbs tested, we identified 12D4 as the most potent inhibitor. 12D4 inhibition of $\alpha\beta$-meATP-evoked inward currents was concentration-dependent with an estimated potency (IC_{50}) of

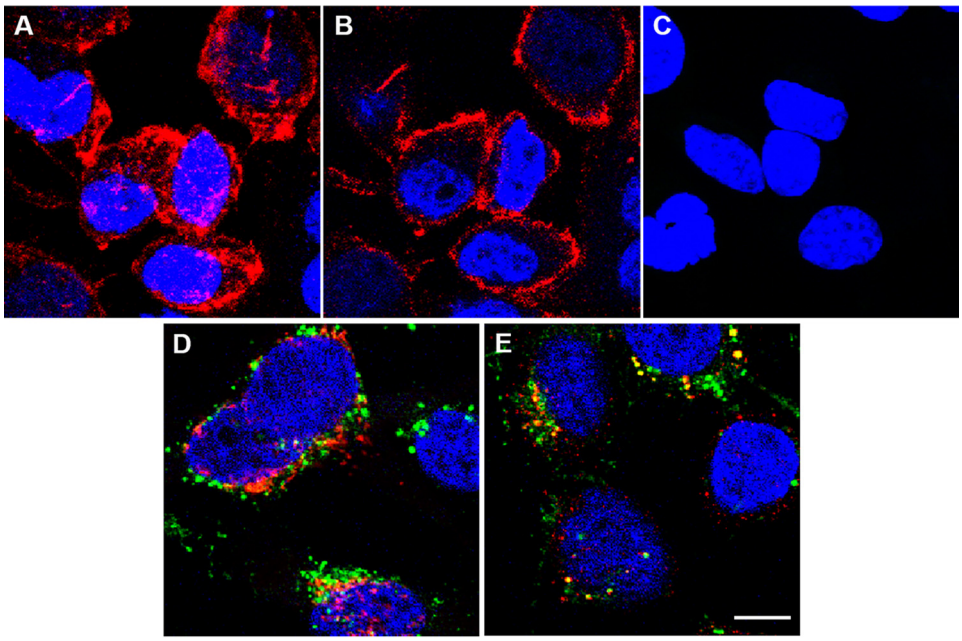

FIGURE 1. **12D4 detects hP2X3 on the plasma membrane and in intracellular organelles.** *A–C*, live cell plasma membrane staining of hP2X3/1321N1 (*A* and *B*) and parental 1321N1 (*C*) cells with 12D4 (*red*) and nuclei (*blue*). Confocal images show maximum projections of *z*-stacks (*A* and *C*) and single *z*-section (*B*). *D* and *E*, intracellular localization of hP2X3. *D* and *E*, 12D4 (*green*) labels organelles that overlap only minimally with the Golgi complex labeled with antibodies against giantin (*red*) (*D*) and partially with early endosomes labeled with antibodies against EEA1 (*red*) (*E*); nuclei are labeled *blue*. Confocal images show single *z*-sections. *Scale bar*, 10 μm.

16 nM (Fig. 2*B*) and showed no detectable effects on activation or inactivation kinetic parameters of hP2X3-mediated currents (Fig. 2*C*).

12D4 Inhibits hP2X3 Receptor-mediated Currents in a State-dependent Manner—Examination of the time course of mAb 12D4 inhibition of $\alpha\beta$-meATP-evoked hP2X3-mediated inward currents revealed that when antibody treatment starts several minutes after the control agonist application, the first post-drug agonist-induced response amplitude was always similar to predrug control or was only slightly inhibited. However, the second and subsequent agonist-induced currents were consistently reduced (Fig. 3*A*). This finding suggests that 12D4 may be acting upon a specific conformational state of hP2X3 receptor. The functional activity of P2X3 receptor in the presence of agonist alone can be described as cycling through three distinct conformational states: resting, activated, and desensitized. Agonist binding triggers the transient opening of P2X3 receptor, which manifests itself as fast inward current followed by quick receptor inactivation and desensitization. In contrast, recovery from desensitization is a relatively slow process; we found that it takes up to 3 min of washout time to gradually restore full agonist response (data not shown). A possible explanation for the phenomenon observed in the presence of 12D4, as represented in Fig. 3*A*, is that the antibody preferentially binds to the receptor in its desensitized state. In order to test this hypothesis, we modified the protocol by shortening the time interval between agonist ($\alpha\beta$-meATP) and antagonist (12D4) applications. In this experiment, 12D4 was applied 20 s after the end of the control agonist pulse. Representative recordings that illustrate the results of the experiment are shown in Fig. 3*B*. In this experimental configuration, the majority of the hP2X3 receptors were in a desensitized state when exposed to 12D4, and the subsequent agonist response was almost maximally inhibited. These results indicate that 12D4 binds to the desensitized conformation of the hP2X3 receptor, possibly locking the receptor in a desensitized state, preventing the normal transition to a resting state.

12D4 Acutely Potentiates the Activity of Recombinant Heteromeric hP2X2/3 Receptors—Like homomeric P2X3 receptors, heteromeric P2X2/3 subtypes are also primarily expressed in nociceptive neurons and play a major role in pain sensation (33). In contrast to P2X3 receptor fast desensitization, P2X2/3-mediated responses display a very slow rate of desensitization (17, 34, 35). We asked whether an hP2X3 antibody would impact the functional activity of heteromeric hP2X2/3 receptors. The 12D4 effects were tested using the automated patch clamp system QPatch with a short term mAb application protocol on human embryonic kidney (HEK 293) cells transiently transfected to express simultaneously both human P2X2 and P2X3 to generate the heterotrimeric hP2X2/3 receptors. In these cells, 12D4 treatments produced a robust potentiation of the slowly desensitizing hP2X2/3-mediated inward currents (Fig. 4*A*). A varying degree of potentiation was observed for only three other mAbs among the 11 mAbs tested (8F4, 24B3, and 8D4) (Fig. 4*B*). The rest of the antibodies induced robust inhibition of the heterotrimeric hP2X2/3 receptor function, with the exception of 9D2 that had no effect upon treatment.

Duration of Exposure to Cells Reveals Two Different Mechanisms of Action of mAbs on hP2X3 and P2X2/3 Receptors—After having examined the modulatory activity of anti-P2X3 mAbs upon short incubation with the cells, we sought to investigate the effect of exposing the cells to the mAbs for several hours (long term treatment). The functional activity of hP2X3 and hP2X2/3 receptors was examined following 20 h of mAb treatment and was compared with the outcome of the 18-min short term treatment. Fig. 5, *A* and *B*, shows the effect of 12D4

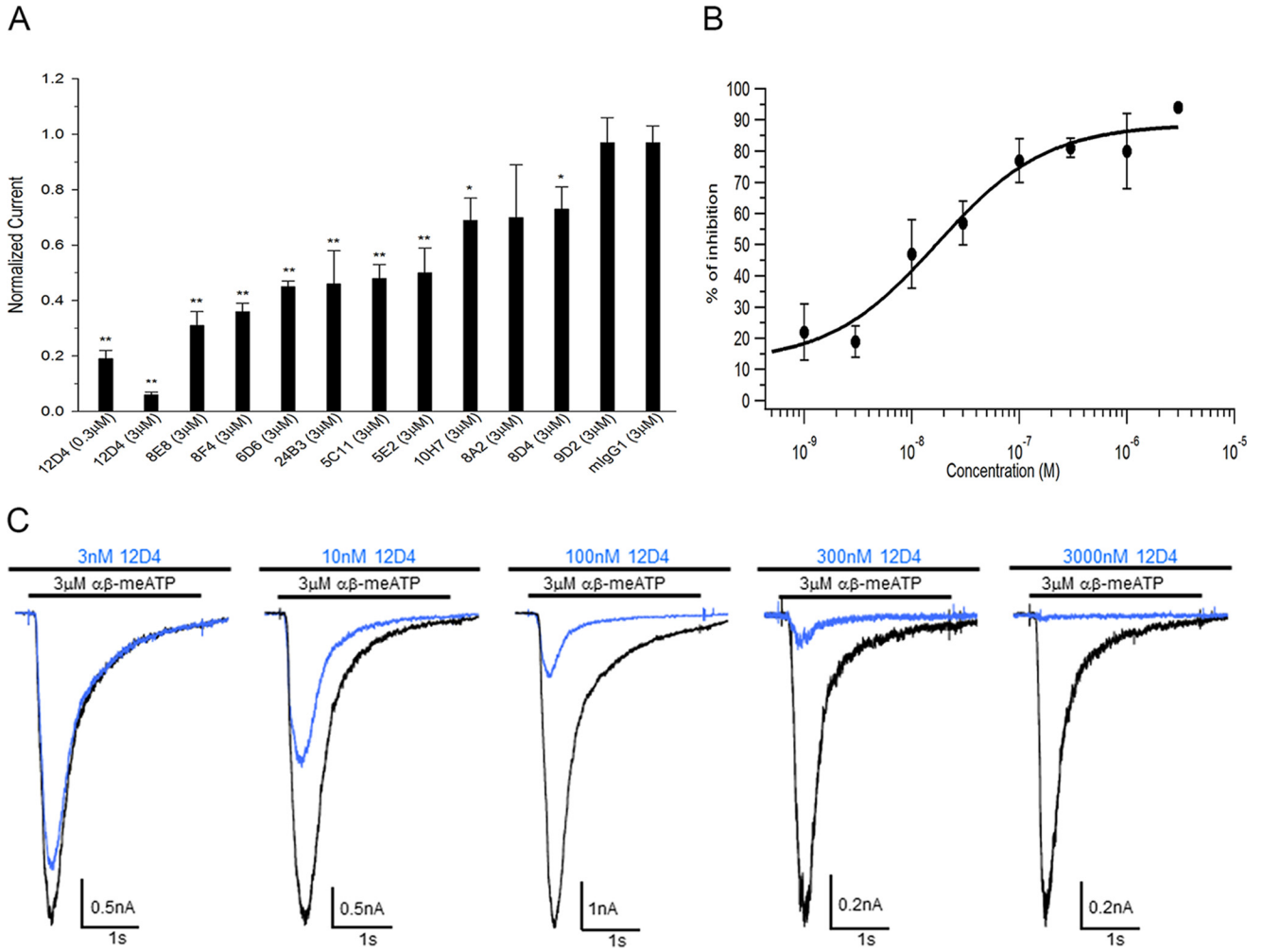

FIGURE 2. **Monoclonal hP2X3 antibodies inhibit hP2X3-mediated currents during short term application.** *A*, bar graph representing inhibitory effects of 11 mAbs on hP2X3-mediated currents. The data are presented as the normalized current calculated as the ratio $I/I_{control}$, where $I_{control}$ is the amplitude of $\alpha\beta$-meATP-evoked inward currents before the antibody application, and I is the current amplitude at the 18-min application time point ($n = 3$–7). *, $p < 0.05$; **, $p < 0.01$. *B*, dose-response relationship for the inhibition of hP2X3-mediated currents by 12D4. The data points were fitted using the Hill equation, giving an IC_{50} of 16.3 ± 10 nM ($n = 3$–10). *C*, representative $\alpha\beta$-meATP-evoked current traces recorded from different hP2X3/1321 cells before (*black*) and after (*blue*) treatment with different concentrations of 12D4. Timing of $\alpha\beta$-meATP and mAb 12D4 applications is indicated by respective *solid black* lines *over* the individual current trace. *Error bars*, S.E.

and 20G6 on $\alpha\beta$-meATP-evoked responses mediated by recombinant hP2X3 receptors after short term (Fig. 5*A*) or long term (Fig. 5*B*) treatments. 20 h of treatment with 12D4 induced a significant additional increase in current inhibition compared with the 18-min short term treatment procedure. 20G6 after short term treatment demonstrated a lack of effect at the concentrations tested (up to 3 μM). In contrast, 20 h of incubation with 20G6 produced a considerable inhibitory effect at 0.3 μM comparable with the effect of 12D4 (Fig. 5*B*).

Furthermore, we found that long term treatment with 12D4 produced a significant inhibition of $\alpha\beta$-meATP-evoked responses mediated by recombinant hP2X2/3 receptors (Fig. 5*D*), in striking contrast to the potentiating effect observed with the short term treatment as shown in Fig. 5*C*. This appeared to be a 12D4-specific effect (*i.e.* epitope-dependent), since 8F4, which also significantly potentiated the hP2X2/3 receptor-mediated inward currents upon short term treatment (Fig. 5*C*), did not show appreciable effects on the $\alpha\beta$-meATP-evoked current amplitude following the long term treatment (Fig. 5*D*). Finally, mAbs such as 10H7 produced consistent robust inhibition of hP2X2/3-mediated currents upon both short and long term treatments.

Collectively, these results suggest that the different antibodies characterized in this study have the ability to modulate the function of P2X receptors in a number of different ways. Inhibition or potentiation of ATP-induced currents is dependent on the homomeric or heteromeric form of the channel and on the duration of its exposure to the antibodies. 12D4, our lead candidate based on its superior blocking activity on both human P2X3 and P2X2/3 upon long term treatment, exemplifies what appears to be two different mechanisms of action, one revealed by a short incubation with the antibody on the order of minutes (short term time course mechanism) and one revealed by a longer incubation on the order of hours (long term time course mechanism). The short term time course mechanism could be explained by antibody binding to the receptor and its direct effect on receptor function, such as blocking conformational changes and ATP binding. For the long term time course mechanism of either greater inhibition by 12D4 or inhibition by mAbs like 20G6, which has no blocking activity upon short

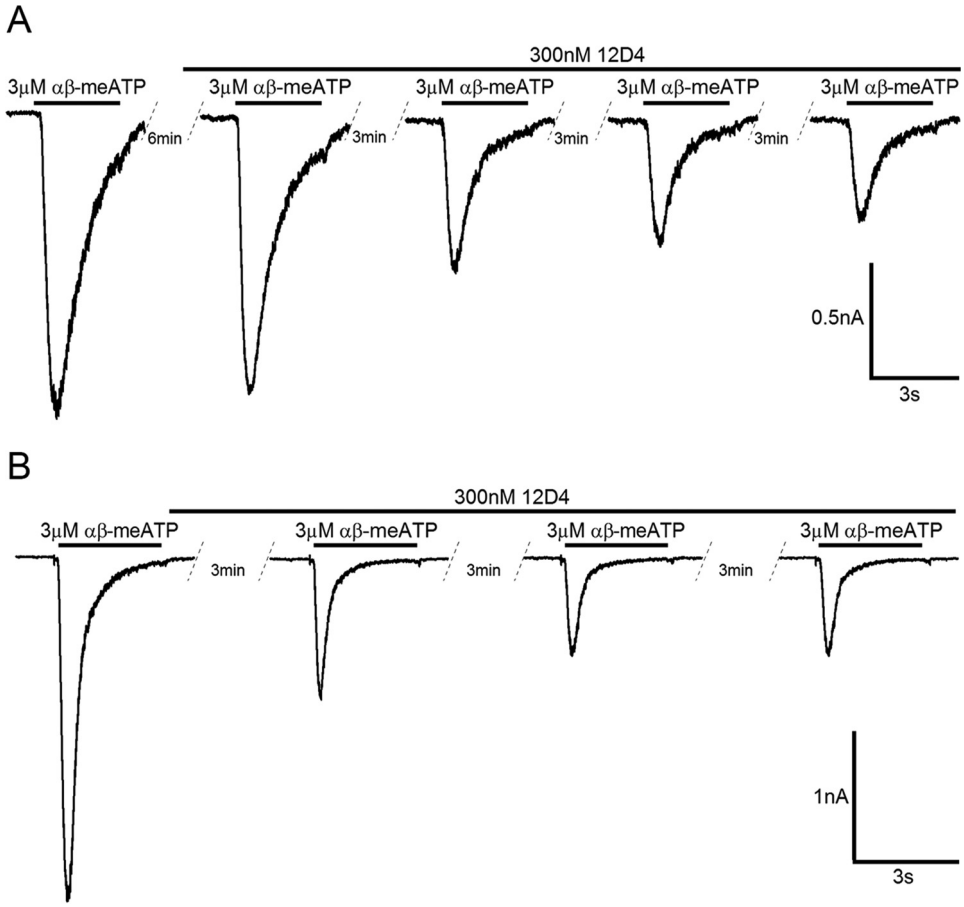

FIGURE 3. **12D4 binds to the desensitized conformation of the hP2X3 receptor.** *A*, representative current traces displaying the time course of changes in peak amplitude of hP2X3-mediated current during 12D4 treatment. Antibody application started 3 min after the end of the initial control $\alpha\beta$-meATP pulse and was maintained through subsequent $\alpha\beta$-meATP pulses at 3-min intervals. The first hP2X3-mediated current in the presence of 12D4 was similar in amplitude to control pretreatment current. Subsequent agonist pulses were significantly decreased in amplitude as indicated ($n = 6$). *B*, decreasing the interval between the end of the $\alpha\beta$-meATP control pulse and the beginning of the application of 12D4 to 20 s resulted in significant inhibition of the first hP2X3-mediated current in the presence of 12D4. Representative recordings in *A* and *B* were made from different hP2X3/1321 cells. Timing of the compound applications is indicated by *solid lines over* the current traces ($n = 12$).

incubation with the receptor, we hypothesized that antibody-induced receptor internalization could be involved (36).

Antibody-mediated Internalization as Inhibitory Mechanism of Action—To investigate the possibility that prolonged (20-h) incubation of antibodies with cells results in antibody-mediated internalization of the channel and therefore in an effective and robust reduction of ATP-stimulated P2X3 currents, we carried out a series of imaging studies using confocal microscopy.

In a first experiment, we incubated 12D4 conjugated to Alexa 488 (12D4-A488) with hP2X3/1321N1 cells on ice for 30 min to allow for antibody binding to the channel on the plasma membrane of cells while minimizing endocytosis. After washing off excess 12D4-A488, the cells were returned to 37 °C to allow endocytosis to occur (Fig. 6, *A–E*). At selected time points, the cells were fixed but not permeabilized, and an anti-Alexa 488 antibody was added to quench the fluorescent signal originating from 12D4-A488 bound to hP2X3 on the plasma membrane; the signal from internalized 12D4-A488 would remain unquenched. The time course clearly indicates that as soon as 15 min and more strongly by 45 min after returning to 37 °C, the cells were internalizing 12D4-A488, bound to hP2X3. No internalization occurred if 12D4-A488 was incubated with the 1321N1 cells that do not express the channel (Fig. 6, *F–J*). Internalized 12D4-A488 accumulated over time in a distinct punctate intracellular compartment. In a complementary experiment, we monitored the disappearance of 12D4 from the plasma membrane of hP2X3/1321N1 cells (Fig. 6, *K–O*). Cells were incubated with unlabeled 12D4 for 30 min on ice, rinsed, and then returned to 37 °C as above. At selected time points, the cells were fixed but not permeabilized, and a secondary fluorescently labeled anti-mouse antibody was added to detect only the 12D4 antibody bound to hP2X3 still on the plasma membrane of the cells. The time course of this experiment showed a strong reduction of plasma membrane staining between the 15- and 45-min time points with even less 12D4 detected by 2 h. These data combined demonstrate that 12D4 internalized and disappeared from the plasma membrane of hP2X3/1321N1 cells with similar kinetics. Although the fact that this did not happen in cells that do not express the channel strongly suggests that the internalization process is dependent on the presence of hP2X3, the data do not formally prove that the antibody actually drives internalization of the channel.

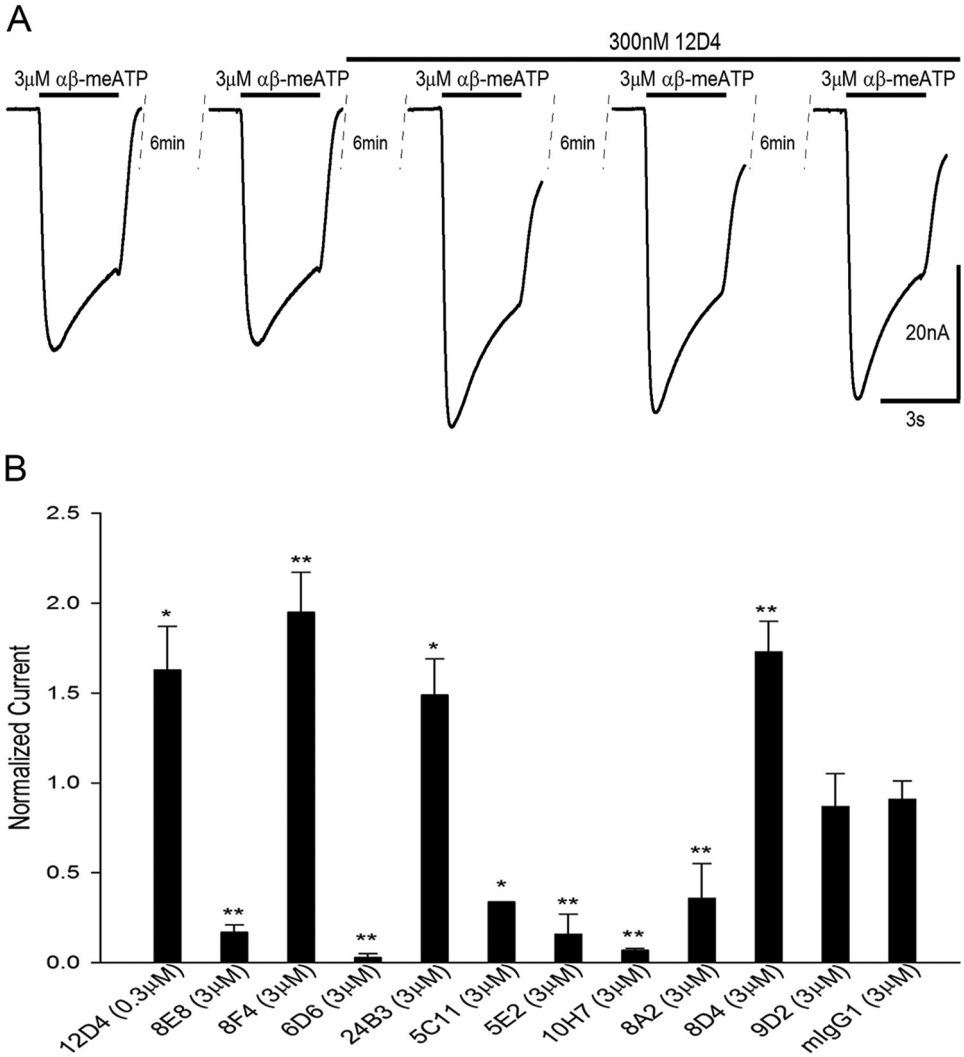

FIGURE 4. **12D4 short term treatment potentiates $\alpha\beta$-meATP-evoked currents mediated by the recombinant heteromeric hP2X2/3 receptor.** *A*, representative current traces displaying the time course of changes in peak amplitude of hP2X2/3-mediated current during 12D4 treatment. Two control agonist applications were followed by 12D4 treatment, resulting in significant potentiation of hP2X2/3-mediated currents ($n = 3$). *B*, bar graph representing the effects of 12 mAbs on hP2X2/3-mediated currents. The data are presented as the normalized current calculated as the ratio $I/I_{control}$, where $I_{control}$ is the amplitude of $\alpha\beta$-meATP-evoked inward currents before the antibody application, and I is the current amplitude at the 18-min Ab application time point ($n = 3$–5). *, $p < 0.05$; **, $p < 0.01$. *Error bars*, S.E.

To gain more definitive evidence that 12D4 drives internalization of hP2X3 after binding to the channel on the plasma membrane of expressing cells, we sought to directly detect the presence, if any, of hP2X3 on the plasma membrane of cells after incubation with 12D4 for 20 h (Fig. 7). 10H7 and 20G6 do not compete with 12D4 for binding to hP2X3 because the staining with one as a directly fluorescently labeled antibody is not significantly affected by the presence of a 10-fold excess of the other as non-labeled antibody (data not shown). When these antibodies were directly labeled with Alexa 488 (10H7-A488 and 20G6-A488, respectively), they detected hP2X3 on the plasma membrane of hP2X3/1321N1 cells (Fig. 7, *A* and *B*, respectively). Cells were incubated for 20 h with 1 μM 12D4 and then fixed but not permeabilized, and 10H7-A488 and 20G6-A488 were added to ascertain the presence of hP2X3 on the plasma membrane of cells. Both antibodies failed to detect any significant amount of channel on the cell surface, demonstrating that overnight incubation with 12D4 efficiently drove its internalization from the plasma membrane (Fig. 7, *C* and *D*, respectively). To further strengthen this conclusion, the addition of a fluorescently labeled anti-mouse antibody to fixed but not permeabilized cells failed to produce any significant cell surface staining, as one would have expected if there had been any 12D4 left bound to hP2X3 still on the plasma membrane after the overnight incubation (Fig. 7*E*). In contrast, if the cells were fixed and permeabilized, allowing for intracellular access of the secondary reagent, the fluorescently labeled anti-mouse antibody detected internalized 12D4 with its characteristic intracellular punctate pattern (Fig. 7*F*).

This strongly suggests that the long term time course mechanism of action of 12D4 is driven by antibody-mediated channel internalization. Next we sought to determine whether 20G6, an antibody demonstrating no activity upon short term treatment but strong inhibitory activity after long term treatment (Fig. 5), also mediated channel internalization. We repeated the internalization experiment detailed above by first

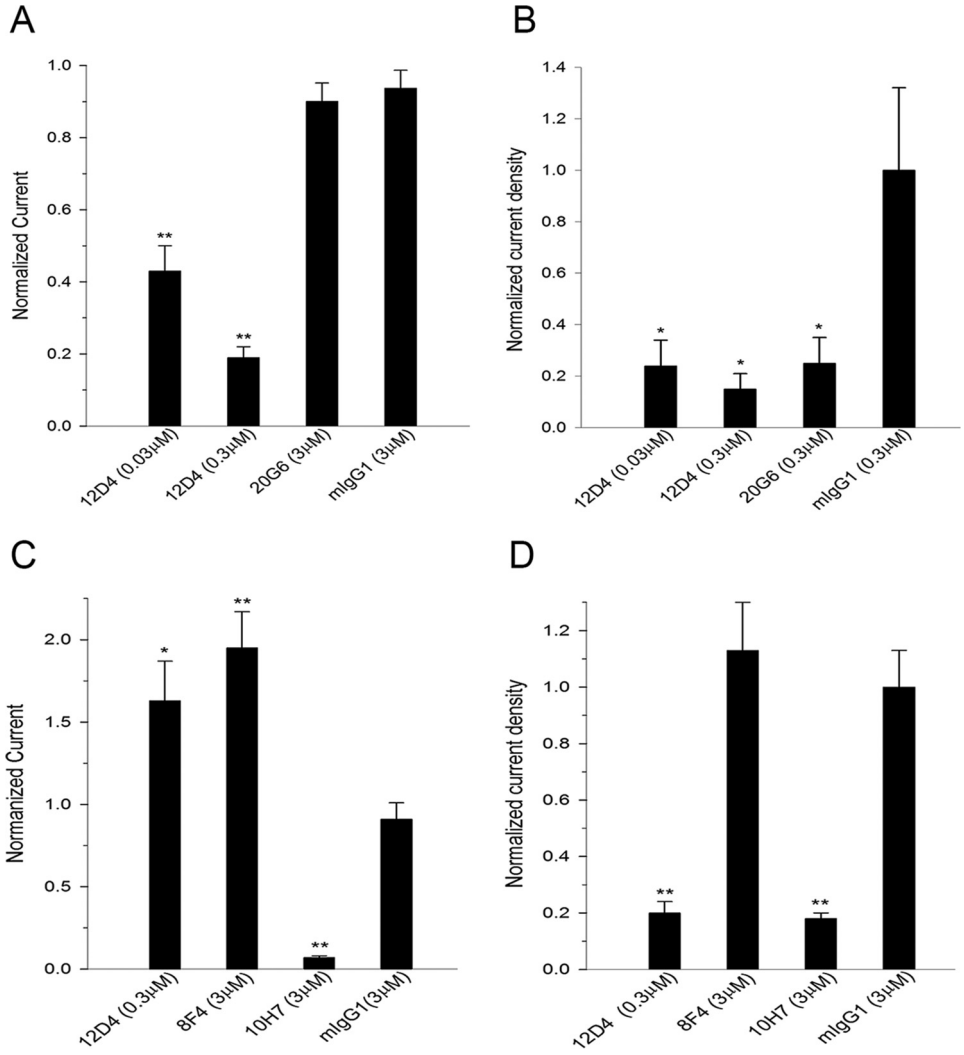

FIGURE 5. **Long term treatment causes effective inhibition of hP2X3-mediated currents by mAbs with opposite acute effects (*A* and *B*) and reverses the potentiating effect of 12D4 on hP2X2/3-mediated current to robust inhibition (*C* and *D*).** *A*, bar graph representing inhibitory effects of 12D4 and 20G6 on hP2X3-mediated currents after short term treatment. The data are presented as the normalized current calculated as the ratio $I/I_{control}$, where $I_{control}$ is the amplitude of $\alpha\beta$-meATP-evoked inward currents before the agonist application, and I is the current amplitude at the 18-min agonist application time point ($n = 4–8$). *, $p < 0.05$; **, $p < 0.01$. *B*, bar graph representing inhibitory effects of 12D4 and 20G6 on hP2X3-mediated currents after long term treatment. The data are presented as the normalized current density calculated as the ratio $I/I_{control}$, where $I_{control}$ is averaged current density in cells treated overnight with nonspecific antibody, and I is averaged current density in cells treated overnight with 12D4 and 20G6 ($n = 6–10$). *, $p < 0.05$; **, $p < 0.01$. *C*, bar graph representing potentiating effects of 12D4 and 8F4 and inhibiting effect of mAb 10H7 on hP2X2/3-mediated currents after short term treatment. The data are presented as the normalized current calculated as the ratio $I/I_{control}$, where $I_{control}$ is the amplitude of $\alpha\beta$-meATP-evoked inward currents before the Ab application, and I is the current amplitude at the 18-min application time point ($n = 3–4$). *, $p < 0.05$; **, $p < 0.01$. *D*, bar graph representing significant inhibitory effects of 12D4, 10H7, and loss of potentiating effect of 8F4 after long term treatment. The data are presented as the normalized current density calculated as the ratio $I/I_{control}$, where $I_{control}$ is averaged current density in cells treated overnight with nonspecific antibody, and I is averaged current density in cells treated overnight with 12D4, 8F4, and 10H7 ($n = 10–11$). *, $p < 0.05$; **, $p < 0.01$. *Error bars*, S.E.

incubating hP2X3/1321N1 cells with 1 μM 20G6 overnight. Cells were then fixed but not permeabilized, and 12D4-A488 and 10H7-A488, both of which do not compete with 20G6 for binding to hP2X3 (data not shown), were used to detect the presence of hP2X3 on the cell surface of the treated cells. Both 12D4-A488 and 10H7-A488 bound to hP2X3 on the surface of cells not incubated with 20G6 (Fig. 8, *A* and *B*, respectively) but failed to detect significant amounts of the channel on the surface of cells exposed to 20G6 for 20 h (Fig. 8, *C* and *D*, respectively). This finding demonstrates that although 20G6 has virtually no acute effect on the activity of hP2X3, its long term incubation with cells can result in a strong inhibition of the ATP-stimulated P2X3 response through efficient removal of the channel from the plasma membrane.

Next we sought to gain additional understanding of the fate of 12D4 and hP2X3 after internalization. To this end, we ran time course experiments of 12D4-A488 internalization in hP2X3/1321N1 cells in conjunction with double labeling with intracellular markers of the endocytic and secretory pathways. hP2X3/1321N1 cells were incubated with 12D4-A488 on ice for 30 min, excess antibody was washed off, and the cells were returned to the 37 °C incubator to initiate the internalization process. At 0.5, 2, 6, and 24 h, the cells were fixed and permeabilized, and antibodies specific for the early endosomal com-

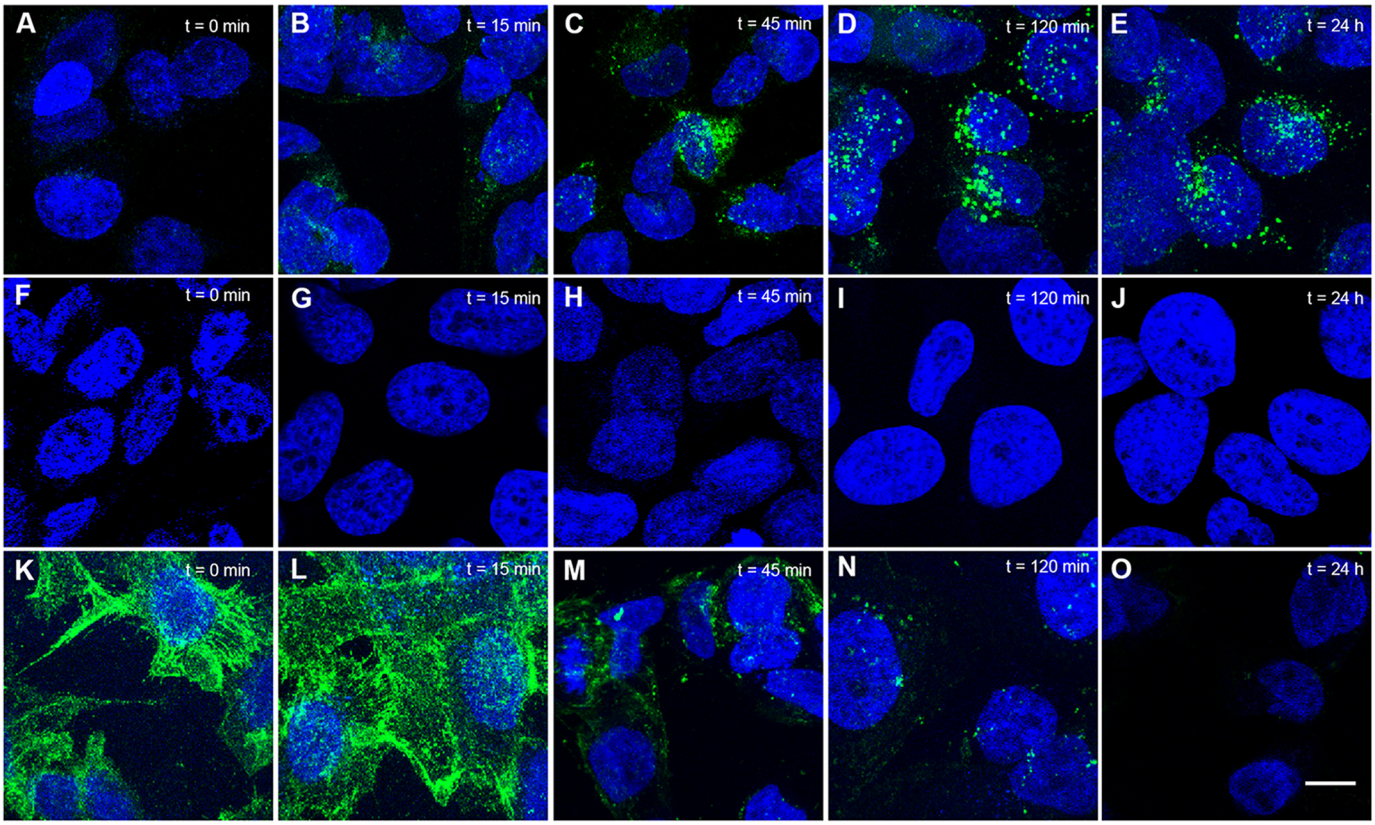

FIGURE 6. **12D4 rapidly internalizes and disappears from the plasma membrane of hP2X3/1321N1 cells.** *A–E*, time course of 12D4-A488 intracellular accumulation in hP2X3/1321N1 cells (*green*); at the indicated time points, cells are fixed but not permeabilized, and the fluorescent signal on the cell surface is quenched with an anti-Alexa 488 antibody. *F–J*, no internalization of 12D4-A488 is observed at any time point if the experiment is done with the parental 1321N1 cells. *K–O*, time course of 12D4 disappearance from the surface of hP2X3/1321N1 cells; at the indicated time points, cells are fixed but not permeabilized, a secondary Alexa 488-conjugated antibody only detects 12D4 on the cell surface (*green*). Nuclei are *labeled blue*. Confocal images show maximum projections of *z*-stacks. *Scale bar*, 10 μm.

partment (EEA1), the lysosomal compartment (cathepsin D), and the Golgi compartment (giantin) were added, followed by an appropriate fluorescently labeled secondary antibody for their detection. Confocal imaging was carried out to determine the relative distribution of internalized 12D4-A488 and its level of co-localization, if any, with the early endosomes, lysosomes, and Golgi complex. Internalized 12D4 partially co-localized with early endosomes from as early as 30 min all the way to 24 h (Fig. 9, *A–C* and *D–F* for the 2- and 24-h time points, respectively; 30 min and 6 h data not shown). Although the overlap is significant, there were clearly organelles that were labeled with 12D4-A488 but did not express the early endosomal marker EEA1, and *vice versa*. Interestingly, the time course of double labeling with the lysosomal marker cathepsin D showed that there is no early co-localization between internalized 12D4 and the lysosomes, but significant overlap was detected at 24 h (Fig. 9, *G–I* and *J–L* for the 2- and 24-h time points, respectively; 30 min and 6 h data not shown). Internalized 12D4-A488 never co-localized with giantin, indicating that there is not an apparent overlap between the early secretory pathway and the P2X3 internalization pathway (Fig. 9, *M–O* and *P–R* for the 2- and 24-h time points, respectively; 30 min and 6 h data not shown). In a final double labeling experiment, we compared the distribution of 12D4-A488 after 2 h of internalization with the distribution of the entire pool of hP2X3 in hP2X3/1321N1 cells using 10H7 conjugated to Alexa 647 (10H7-A647) after cell fixation and permeabilization. Because 10H7-A647 does not compete with 12D4 for binding to hP2X3, it was expected to label both the pool of hP2X3 that had been internalized from the plasma membrane and was probably still bound to 12D4 and the steady-state intracellular pool of hP2X3 (Fig. 10). The data showed significant intracellular punctate co-localization of the 12D4-A488-generated fluorescent signal with the signal for total hP2X3 produced by 10H7-A647 binding, indicating that 12D4 does indeed travel together with hP2X3 from the plasma membrane or that at the very least internalized 12D4-A488 ends up in a compartment populated with hP2X3.

A thorough understanding of the mechanism of action of the investigational antibodies has obvious important implications for designing appropriate preclinical animal studies and interpretation of results. Likewise, *ex vivo* evaluation of the antibodies' affinity and potency on primary cells or on exogenously expressed targets from animal species of choice is usually the prerequisite for subsequent preclinical *in vivo* studies. Therefore, we next examined the effects of 12D4 on rodent P2X3 and P2X2/3 receptors.

Anti-hP2X3 mAbs Dose-dependently Inhibit Recombinant Rat P2X3 Receptors and Native Rodent P2X3-mediated Currents—Antibody cross-reactivity between species is often beneficial because it allows the use of the clinical lead Ab in preclinical animal models. There is a high degree of amino acid sequence homology between human and rat P2X3 receptors

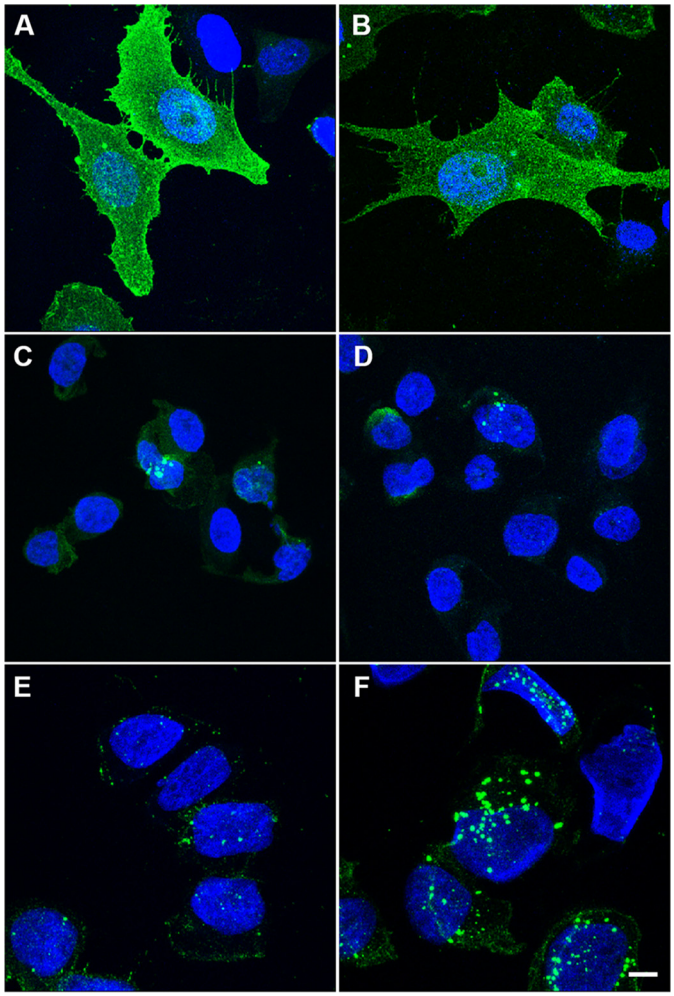

FIGURE 7. **12D4 drives internalization of hP2X3.** *A* and *B*, 10H7-A488 and 20G6-A488 (*green*) detect hP2X3 on the plasma membrane of hP2X3/1321N1 cells, respectively. *C* and *D*, following overnight incubation with 1 μM 12D4, 10H7-A488 and 20G6-A488, respectively, do not detect any hP2X3 on the cell surface of the cells. *E*, an Alexa 488-conjugated secondary antibody added after overnight incubation of cells with 1 μM 12D4 also does not detect any 12D4 on the cell surface. *F*, the intracellularly accumulated 12D4 is readily detected. Nuclei are labeled *blue*. Cells are fixed but not permeabilized (*A–E*) or fixed and permeabilized (*F*) before detection of hP2X3 (*A–D*) or 12D4 with a secondary antibody (*E* and *F*). Confocal images show maximum projections of *z*-stacks. *Scale bar*, 10 μm.

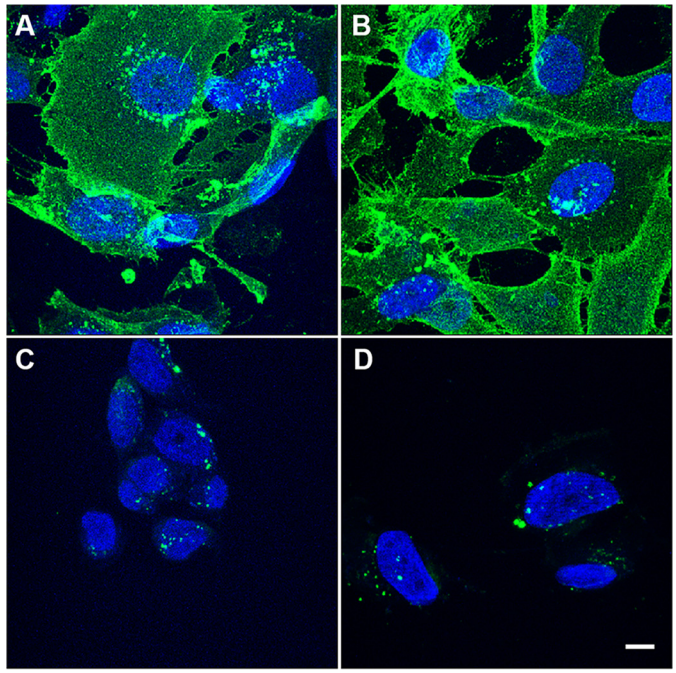

FIGURE 8. **20G6 drives internalization of hP2X3.** *A* and *B*, 12D4-A488 and 10H7-A488 detect hP2X3 on the plasma membrane of hP2X3/1321N1 cells, respectively. *C* and *D*, following overnight incubation with 1 μM 20G6, no hP2X3 is detected by 12D4-A488 or 10H7-A488, respectively, on the cell surface of hP2X3/1321N1 cells. Nuclei are labeled *blue*. Cells are fixed but not permeabilized before detection of hP2X3. Confocal images show maximum projections of *z*-stacks. *Scale bar*, 10 μm.

(93% identity) (37), which makes it plausible to expect functional activity of anti-hP2X3 Abs against the rat P2X3 receptor. To test this possibility, a human glial cell line 1321N1 stably expressing recombinant rat P2X3 receptors was used. The panel of 11 anti-hP2X3 mAbs evaluated previously on human P2X3 receptors (Fig. 2*A*) was found to be appreciably less potent in blocking rat P2X3-mediated currents (Fig. 11*A*). The inhibitory effect of 12D4, in particular, was significantly weaker on recombinant rat P2X3 receptors, producing only ~60% current block at 3 μM, the highest concentration tested (Fig. 11*B*), with no effect on activation and desensitization kinetics of the rat P2X3-mediated currents (data not shown). However, in overnight incubation experiments on recombinant rat P2X3 receptors, 12D4 appeared to be more potent, inducing ~60% current block at 100 nM and ~70% current block at 200 nM (Fig. 11*C*).

Manual patch clamp recording from cultured rat dorsal root ganglion neurons was employed to confirm the functional effect of 12D4 on native rodent P2X receptors. It is well established that these sensory neurons endogenously express a diverse population of P2X receptors (38, 39). For the P2X3 subtype in particular, it has been shown that corresponding mRNA is abundantly and selectively localized in sensory neurons, including those of dorsal root (DRG) and trigeminal and nodose ganglia (15–17). The P2X3 receptor's current has distinctive fast activation kinetics, and it desensitizes rapidly in the continued presence of agonist (17, 40). P2X1 receptors also display a similar kinetic profile; therefore, one should be careful not to assume that ATP-induced currents with the fast kinetic profile in DRG neurons are mediated exclusively by P2X3 receptors (41). However, a considerable body of data indicates that the P2X1 expression is lowest among other P2X receptors in sensory neurons (7, 42), which would indicate that the P2X3 receptors predominantly mediate ATP-induced fast inactivating currents in rat DRG neurons.

In our electrophysiological experiments on cultured adult rat small diameter DRG neurons, $\alpha\beta$-meATP-evoked inward currents with the kinetic profile of a P2X3-mediated response were detected in ~80% of tested cells. These putative P2X3-mediated currents were potently inhibited by 12D4 in a concentration-dependent manner, displaying 58.8 ± 6.6% ($n = 4$) current block at 150 nM (Fig. 12, *A* and *C*), 61 ± 3.2% ($n = 8$) current block at 300 nM (data not shown), and 71% current block at 480 nM ($n = 1$) (Fig. 12, *B* and *D*). The inhibitory effect of 12D4 was almost irreversible because only an insignificant amount of current amplitude recovered during the 20-min wash-out phase (Fig. 12, *A–D*).

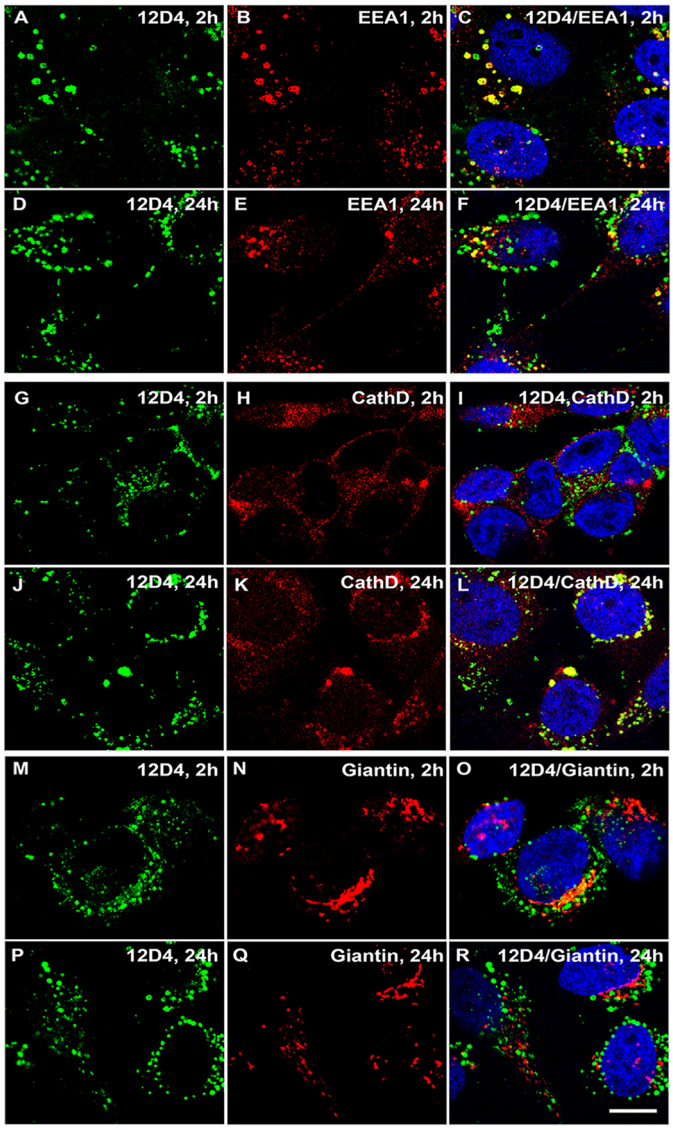

FIGURE 9. **Internalized 12D4 accumulates in organelles that partially overlap with early endosomes first and with lysosomes later.** hP2X3/1321N1 cells were incubated with 12D4-A488, and the subcellular localization of internalized antibody was investigated at 2 and 24 h by double labeling with markers of early endosomes, lysosomes, and the Golgi complex. *A–F*, double labeling of 12D4-A488 (*green*, *A* and *D*) with the early endosomal marker EEA1 (*red*, *B* and *E*) with overlaid images showing partial overlap (*yellow*, *C* and *F*) at both 2 h (*A–F*) and 24 h (*D–F*). *G–L*, double labeling of 12D4-A488 (*green*, *G* and *J*) with the lysosomal marker cathepsin D (*red*, *H* and *K*) with overlaid images showing partial overlap (*yellow*, *C* and *F*) at 24 h (*J–L*) but not at 2 h (*G–I*). *M–R*, double labeling of 12D4-A488 (*green*, *M* and *P*) with the Golgi complex marker giantin (*red*, *N* and *Q*) with overlaid images showing no overlap (*O* and *R*) at 2 h (*M–O*) and 24 h (*P–R*). Nuclei are labeled *blue*. Confocal images show single *z*-sections. *Scale bar*, 10 μm.

Analysis of the time course of 12D4 inhibition of $\alpha\beta$-meATP-evoked inward currents in rat DRG neurons confirmed the previous findings that the antibody binds to the inactivated state of the P2X3 channel (Fig. 12, *A* and *B*).

12D4 Potentiates Native Rat P2X2/3 Receptor-mediated Currents—In our experiments on adult rat DRG small diameter neurons, ~15% of $\alpha\beta$-meATP-evoked inward currents displayed a mixed fast and slow time course of desensitization or a pure slow desensitization kinetic. This slow kinetic of current desensitization is a distinct hallmark of heterotrimeric P2X2/3-mediated responses (17, 33, 34). Similar to the observed potentiating effect of 12D4 on recombinantly expressed human P2X2/3 receptors in 1321N1 cells, 12D4 treatments produced a robust potentiation of the slowly desensitizing $\alpha\beta$-meATP-evoked inward currents in rat DRG neurons (Fig. 12, *E* and *F*). In a total of four different cells displaying slow desensitizing $\alpha\beta$-meATP-evoked currents, we observed a 227 and 228% current amplitude increase at 150 nM 12D4 (Fig. 12, *E* and *F*), 205% current amplitude increase at 230 nM 12D4 (data not shown), and 380% current amplitude increase at 330 nM 12D4 (data not shown). The potentiating effect of 12D4 was fully reversible upon antibody wash-out (*i.e.* the P2X2/3-mediated current returned to the pretreatment amplitude in about 15 min) (Fig. 12, *E* and *F*). It can be noticed in Fig. 12*E* that the agonist-induced control current before 12D4 application clearly combines the fast and the slow inactivating component. Upon 12D4 application and after wash-out, the fast inactivating component is abrogated, consistent with the irreversible inhibitory effect of 12D4 on the fast inactivating P2X3-mediated current.

Taken together, these *in vitro* data demonstrate that 12D4 blocks the activity of recombinant and native rat P2X3 receptors upon short term treatment, albeit with reduced potency compared with the activity on human P2X3. Most importantly, long term treatment with 12D4 produces a strong blocking effect on rat P2X3, allowing for its meaningful testing in animal models of pain conditions.

In Vivo Effects of 12D4—To establish the *in vivo* relevance and therefore therapeutic potential of P2X3 function-blocking antibodies, we examined the effects of 12D4 in rodent models of visceral pain, inflammatory pain, and formalin-induced pain.

12D4 Reverses Visceral Pain—To test for effects involving visceral pain, a TNBS-induced visceral hypersensitivity rat model was used. In this model, 7 days postsurgery, rats treated with IgG control (30 mg/kg) 3 days before colonic balloon distension exhibited a 37% reduction (24.2 ± 2.6 mm Hg, $p < 0.05$ compared with sham; Fig. 13*A*) in threshold tolerance compared with untreated sham surgery rats (100%, 38.2 ± 4.6 mm Hg). Rats treated with 12D4 (30 mg/kg) 3 days before balloon distension exhibited a 63% recovery of threshold (33.0 ± 2.2 mm Hg, $p < 0.05$ compared with IgG control; Fig. 13*A*).

12D4 Shows No Effect on Inflammatory Pain—To investigate whether 12D4 had any effect on inflammatory pain, we tested paw withdrawal latency in response to radiant heat in a CFA-induced model of inflammatory pain in the rat. Subcutaneous administration of IgG control or 12D4 3 days before CFA-induced inflammation did not significantly affect the thermal response latencies tested either before or 48 h after CFA-induced inflammation (Fig. 13*B*).

12D4 Shows No Effect in Formalin Test—We used a 0.5% intraplantar formalin injection to test for effects of 12D4. Three days before formalin injection, rats were injected subcutaneously with either vehicle (PBS) or 12D4 (30 mg/kg). No difference was seen in the number of flinches observed between the treatment groups during the 60 min of observation (Fig. 13, *C* and *D*).

Discussion

Effective management of chronic pain conditions continues to represent an unmet medical need, and there is a need for

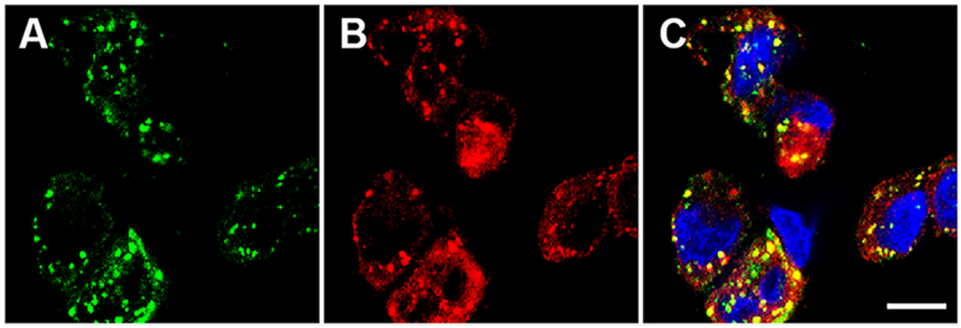

FIGURE 10. **Internalized 12D4 accumulates in organelles that also contain hP2X3.** *A* and *B*, internalized mAb 12D4-Alexa 488 (*green*, *A*) accumulates in organelles that also harbor hP2X3 as detected by 10H7-Alexa 647 (*red*, *B*). *C*, the overlay shows significant areas of overlap in *yellow*. Nuclei are labeled *blue*. Confocal images show single *z*-sections. *Scale bar*, 10 μm.

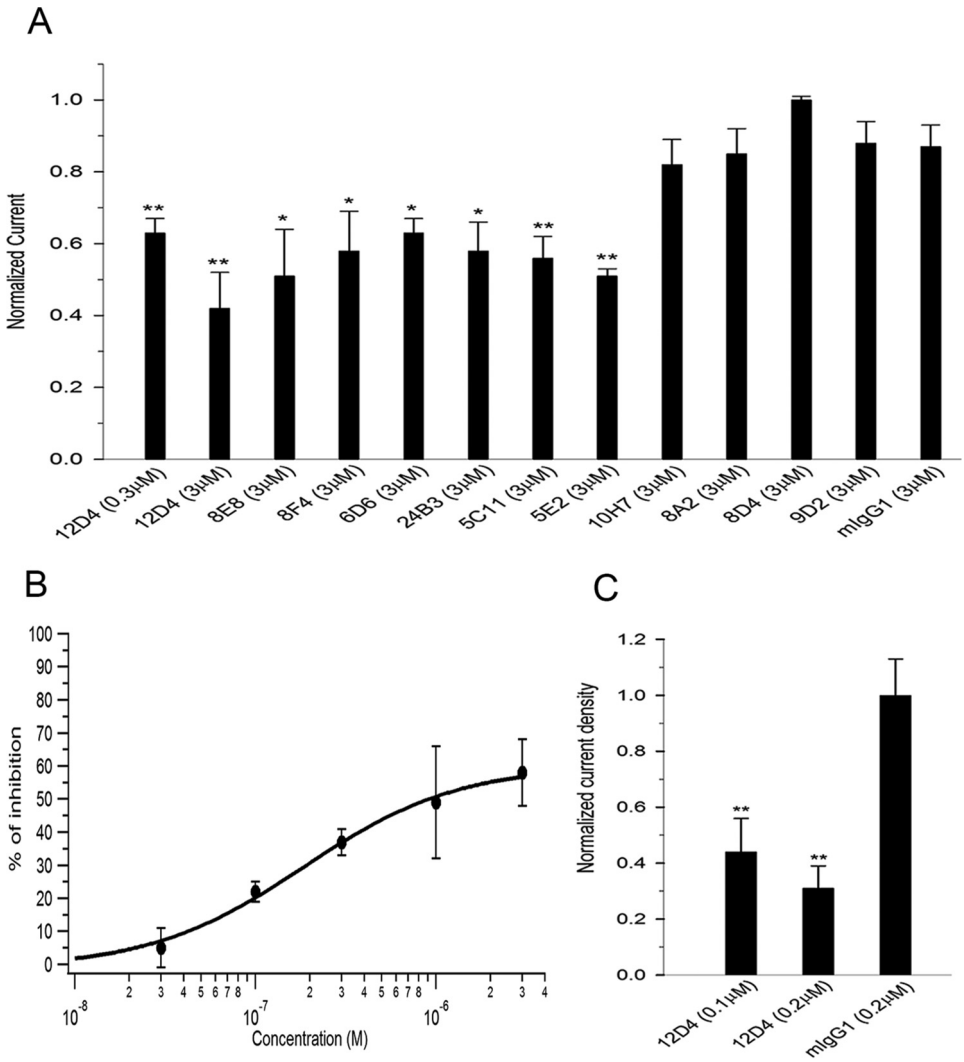

FIGURE 11. **Monoclonal hP2X3 antibodies inhibit recombinant rat P2X3 receptors during short term and long term agonist application.** *A*, bar graph representing inhibitory effects of 11 mAbs on recombinant rat P2X3-mediated currents. The data are presented as the normalized current calculated as the ratio $I/I_{control}$, where $I_{control}$ is the amplitude of $\alpha\beta$-meATP-evoked inward currents before the Ab application, and I is the current amplitude at 18 min after Ab application ($n = 3–6$). *, $p < 0.05$; **, $p < 0.01$. *B*, the dose-response relationship for the inhibition of recombinant rat P2X3-mediated currents by 12D4. The data points were fitted with the Hill equation, giving an IC_{50} of 185.5 $\pm$ 41.7 ($n = 3–5$). *C*, bar graph representing inhibitory effects of 12D4 on recombinant rat P2X3-mediated currents after long term treatment. The data are presented as the normalized current density calculated as the ratio $I/I_{control}$, where $I_{control}$ is averaged current density in cells treated overnight with nonspecific antibody, and I is averaged current density in cells treated overnight with 12D4 ($n = 13–19$). *, $p < 0.05$; **, $p < 0.01$. *Error bars*, S.E.

additional efficacious analgesics with better safety profiles. The purinergic ATP-gated ion channels P2X3 and P2X2/3 are involved in nociceptive signaling, and their therapeutic targeting with small molecule antagonists has shown promise in the clinic. We chose to investigate antibodies as an alternative to small molecules targeting P2X3 and P2X2/3. Therapeutic anti-

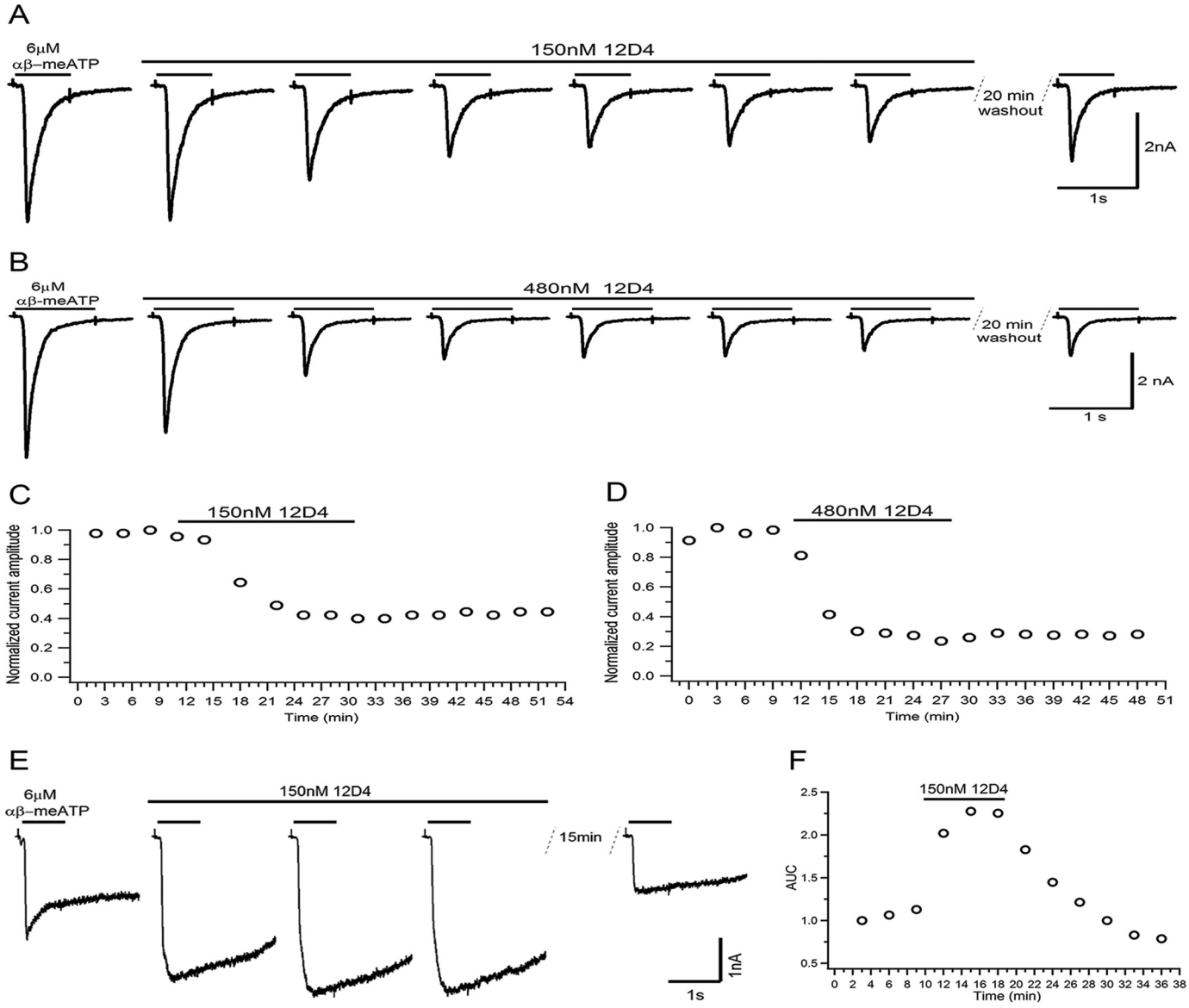

FIGURE 12. **12D4 inhibits $\alpha\beta$-meATP-evoked rapidly desensitizing currents and potentiates $\alpha\beta$-meATP-evoked slowly desensitizing currents in adult rat small diameter DRG neurons.** *A* and *B*, representative current traces displaying the time course of the changes in the peak amplitude of $\alpha\beta$-meATP-evoked rapidly desensitizing currents recorded from rat small diameter DRG neurons during treatment with 150 nM ($n = 4$) and 480 nM ($n = 1$) 12D4, respectively. The time of the compound application is indicated by the *solid line over* the current traces. *C* and *D*, the entire time course of the changes in the peak amplitude of $\alpha\beta$-meATP-evoked currents in rat small diameter DRG neurons from the recordings partially presented in *A* and *B*, respectively. Data are presented as normalized peak current amplitude *versus* time (minutes). The time of the compound application is indicated by a *solid line*. *E*, representative current traces displaying the time course of the changes in the amplitude of $\alpha\beta$-meATP-evoked slowly desensitizing current recorded from a rat small diameter DRG neuron during 150 nM 12D4 treatment. The time of the compound application is indicated by a *solid line over* the current traces ($n = 2$). *F*, the entire time course of the changes in the amplitude of $\alpha\beta$-meATP-evoked slowly desensitizing current in rat small diameter DRG neuron from the recording partially presented in *E*. Data are presented as normalized area under the curve (*AUC*) *versus* time (minutes). The time of the compound application is indicated by a *solid line*.

bodies, as an alternative to small molecule-based drugs, are increasingly utilized for the treatment of diseases, due to their remarkable specificity toward their targets and their favorable pharmacokinetics properties (26).

Here we describe a panel of anti-humanP2X3 antibodies that modulates the function of homomeric P2X3 receptors and heteromeric P2X2/3 receptors in a number of distinct ways, depending on the duration of antibody exposure to the channels. Differences in binding affinity and, perhaps more importantly, in binding epitope are probably at the base of the different effects that these antibodies have on the activity of these channels. First, using whole-cell patch clamp recording, we have revealed an acute effect of the antibodies by demonstrating a quick onset upon application. Second, whereas all of the antibodies tested displayed various degrees of inhibition on the homomeric hP2X3 channel (Fig. 2*A*), some mediated inhibition, and some, unexpectedly, mediated potentiation of the heteromeric P2X2/3 activity (Fig. 4*B*). Specifically, mAb 12D4 potently inhibited the activity of P2X3 channels yet significantly potentiated P2X2/3 receptor-mediated currents. The endogenous steroid dehydroepiandrosterone (43, 44) and the inflammatory mediators substance P and bradykinin can

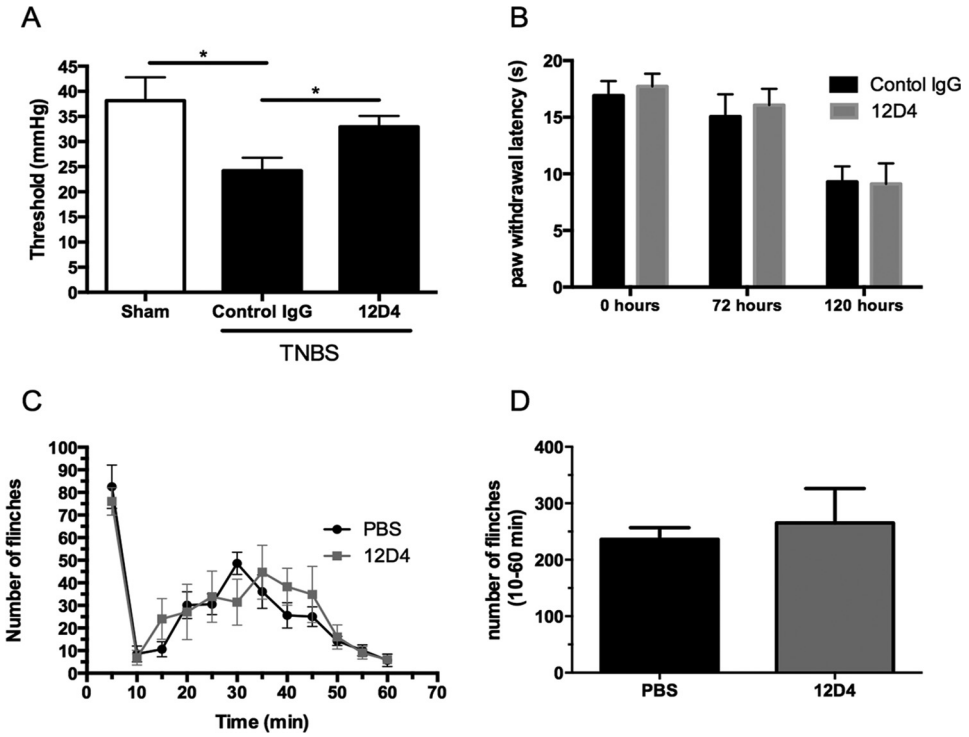

FIGURE 13. ***In vivo* effects of 12D4.** *A*, 12D4 is efficacious in a TNBS-induced colitis model. Seven days after colonic TNBS exposure, rats were tested for a threshold pain response to colonic balloon distension and compared with thresholds of sham-operated rats (38.2 ± 4.6 mm Hg, $n = 5$). Rats treated with control IgG (30 mg/kg) 3 days before balloon distension exhibited a 37% reduction in threshold (24.2 ± 2.6 mm Hg, $p < 0.05$, $n = 15$, compared with sham). Rats treated with 12D4 (30 mg/kg) 3 days before balloon distension exhibited a 63% recovery of threshold (33.0 ± 2.2 mm Hg, $p < 0.05$, $n = 19$, compared with IgG control). One-way analysis of variance with Dunnett's multiple comparisons test was used. *B*, 12D4 shows no effect on inflammatory pain in a CFA model. Three days before CFA injection, animals were tested for baseline withdrawal latency to a noxious thermal stimulus (0 h) and then received treatment (control IgG or 12D4 (30 mg/kg subcutaneously)). Withdrawal latencies to noxious thermal stimulus were again tested (72 h) before CFA injection and 48 h after CFA injection (120 h). Withdrawal latency was reduced post-CFA injection. No difference was seen between treatment groups ($n = 10$/group). *C* and *D*, 12D4 shows no effect in a 0.5% formalin model. Three days before testing, female rats received either PBS (vehicle) or 12D4 (30 mg/kg subcutaneously). On the day of testing 50 μl of 0.5% formalin was injected into the plantar surface of the left hind paw. Painlike behavior (persistent flinching) of the injected paw was manually recorded (number of flinches/5-min interval) for 60 min (*C*). No difference was seen between treatment groups in total number of flinches recorded from 10 to 60 min (*D*). $n = 8$ (PBS), and $n = 7$ (12D4). *, $p < 0.05$. *Error bars*, S.E.

induce a similar fast potentiation of P2X2/3-mediated currents by induction of a remarkable decrease of the desensitization rate (45). In contrast, we found that 12D4-induced potentiation of the P2X2/3 current occurred without an apparent decrease in the desensitization rate (Fig. 4*A*). This suggests a different mechanism underlying the 12D4-mediated potentiation of the P2X2/3 channel. Third, our findings indicate that the acute inhibitory effect of 12D4 on hP2X3 currents occurs when the antibody binds to the desensitized P2X3 receptors (Fig. 3). Interestingly, a similar state-dependent inhibitory effect on P2X3 currents has been reported for purotoxin-1, a peptide from spider venom (46). Previous published P2X3 studies have postulated the existence of a high affinity desensitized state of the receptor (47). The slow rate of agonist release from the high affinity desensitized state essentially locks the receptor in the desensitized state (47). We hypothesize that 12D4 can similarly stabilize the desensitized state of the P2X3 receptor. Further studies on the receptor epitope for the antibody will be required to elucidate this.

Finally, and more importantly in light of a possible therapeutic application of these antibodies, we found that prolonging antibody exposure for hours invariably resulted in a greater inhibitory effect on homomeric hP2X3 channels for all of the antibodies and even robust reversal of the potentiating effect on P2X2/3 receptors (Fig. 5).

In a series of imaging experiments, we showed that both antibodies with prominent acute inhibitory activity, such as 12D4, and antibodies with minimal effect upon short exposure to the channel, such as 20G6, drove rapid and efficient internalization of hP2X3 from the plasma membrane of expressing cells (Figs. 6–8). Co-localization of internalized 12D4 with markers of intracellular organelles demonstrated trafficking to early endosomes first and to lysosomes later, suggesting a mechanism of antibody-mediated internalization and lysosomal targeting for degradation (Figs. 9 and 10). The functional activity of members of the P2X receptor family is modulated by their trafficking properties and by their subcellular distribution. The dynamics of cellular trafficking and targeting differs among the P2X receptors and is dependent on interactions with ligands, regulatory molecules, and lipids (48). P2X3 undergoes rapid constitutive internalization and is predominantly localized to late endosomes and lysosomes with a minor population present at the plasma membrane (49). ATP stimulation induces an increase in channel density at the plasma membrane of primary sensory neurons in a process driven by CaMKIIα and caveolin-1 (49, 50). Similarly, it has been shown that exposure of trigeminal sensory neurons to CGRP results in increased trafficking of P2X3 to the cell surface (51). Overall, our data fit well with the reported subcellular distribution of P2X3 and its trafficking dynamics. We suggest that antibody binding to the

channel on the cell surface promotes efficient internalization and lysosomal targeting by using intracellular trafficking pathways that partially overlap with those used by the cells to modulate receptor activity.

We next sought to test these antibodies and 12D4 in particular in rodent animal models of pain. Therefore, we first determined their activity on exogenously expressed rat P2X3 receptors and on native purinergic receptors in rat DRG neurons. We found that despite the fact that the activity of 12D4 on rat P2X3 is significantly lower with the short term treatment (Figs. 11 (*A* and *B*) and 12 (*A*–*D*)) compared with human P2X3 receptors (Fig. 2*A*), its activity with the long term treatment revealed greater cumulative blocking effect (Fig. 11*C*), making the testing in rodent animal models of pain relevant.

The anti-hyperalgesic approach of P2X3 antagonism with small molecules like A-317491 has been validated in common rodent models of pain, such as the formalin model of persistent pain and the CFA-induced thermal hyperalgesia model (52) and in multiple models of visceral pain (13, 52, 53). We therefore chose to test 12D4 in the formalin and CFA models and a model of visceral hypersensitivity representative of the hallmarks of irritable bowel syndrome (54). 12D4 treatment was effective in partially restoring threshold responses compared with control in the visceral hypersensitivity model but failed to show any difference from control treatment in either the formalin model or the CFA model. There may be multiple explanations for why 12D4 did not show efficacy in the models where antagonists such as A-317491 did (52, 55). Efficacy in the visceral hypersensitivity model confirmed that our choice of 30 mg/kg, 3 days before testing, was a valid dosing approach. The CFA model was dosed 30 mg/kg, 3 days before CFA injection, which was still 5 days before the thermal hypersensitivity testing. This was necessary to confirm that 12D4 dosing did not change the baseline response to the noxious thermal stimulus before the CFA-induced inflammation. It is possible that this additional 2 days was sufficient time to clear 12D4 to sub-efficacious levels. Dosage and timing in the formalin model study was similar to what was done in the visceral hypersensitivity study and therefore not the likely explanation for the lack of effect in this model. Procedural differences from the published models may account for the formalin model results. We used a 0.5% formalin concentration *versus* the 5% formalin used by Jarvis *et al.* (52). Different concentrations of formalin have been suggested to activate different populations of sensory neurons in this model (56), which could account for the differences from published results. Obviously, further work is required to understand the difference in results published for A-317491 in the formalin and CFA models *versus* what our results demonstrate. The fact that 12D4 is effective at reversing TNBS-induced visceral hypersensitivity is consistent with assertions that P2X3 antagonism is indicated for clinical chronic visceral pain treatment (13). An antibody-based approach to visceral pain treatment could provide an alternative to small molecule therapeutics, with a differing profile of dosing and potential side effects. Our data suggest that a humanized version of 12D4 could be a therapeutic for irritable bowel syndrome and other visceral pain indications.

Author Contributions—A. S., D. F., K. P., P. S., A. R., and D. S. conceived and coordinated the study and wrote the paper. G. Z., A. H.-M., J. M. W., C. L., S. K., A. P., J. Y., C. B., J. K. L., and R. S. provided technical assistance in acquisition of data and contributed to the analysis and interpretation of data. All authors reviewed the results and approved the final version of the manuscript.

References

1. Burnstock, G. (2014) Purinergic signalling: from discovery to current developments. *Exp. Physiol.* **99,** 16–34
2. North, R. A. (1996) P2X purinoceptor plethora. *Semin. Neurosci.* **8,** 187–195
3. Lewis, C., Neidhart, S., Holy, C., North, R. A., Buell, G., and Surprenant, A. (1995) Coexpression of P2X2 and P2X3 receptor subunits can account for ATP-gated currents in sensory neurons. *Nature* **377,** 432–435
4. Jiang, L. H., Kim, M., Spelta, V., Bo, X., Surprenant, A., and North, R. A. (2003) Subunit arrangement in P2X receptors. *J. Neurosci.* **23,** 8903–8910
5. Kawate, T., Michel, J. C., Birdsong, W. T., and Gouaux, E. (2009) Crystal structure of the ATP-gated P2X4 ion channel in the closed state. *Nature* **460,** 592–598
6. Hattori, M., and Gouaux, E. (2012) Molecular mechanism of ATP binding and ion channel activation in P2X receptors. *Nature* **485,** 207–212
7. Burnstock, G., and Knight, G. E. (2004) Cellular distribution and functions of P2 receptor subtypes in different systems. *Int. Rev. Cytol.* **240,** 31–304
8. Jarvis, M. F., and Khakh, B. S. (2009) ATP-gated P2X cation-channels. *Neuropharmacology* **56,** 208–215
9. Burnstock, G. (2013) Purinergic mechanisms and pain: an update. *Eur. J. Pharmacol.* **716,** 24–40
10. Barclay, J., Patel, S., Dorn, G., Wotherspoon, G., Moffatt, S., Eunson, L., Abdel'al, S., Natt, F., Hall, J., Winter, J., Bevan, S., Wishart, W., Fox, A., and Ganju, P. (2002) Functional downregulation of P2X3 receptor subunit in rat sensory neurons reveals a significant role in chronic neuropathic and inflammatory pain. *J. Neurosci.* **22,** 8139–8147
11. Kaan, T. K., Yip, P. K., Patel, S., Davies, M., Marchand, F., Cockayne, D. A., Nunn, P. A., Dickenson, A. H., Ford, A. P., Zhong, Y., Malcangio, M., and McMahon, S. B. (2010) Systemic blockade of P2X3 and P2X2/3 receptors attenuates bone cancer pain behaviour in rats. *Brain* **133,** 2549–2564
12. Ye, Y., Ono, K., Bernabé, D. G., Viet, C. T., Pickering, V., Dolan, J. C., Hardt, M., Ford, A. P., and Schmidt, B. L. (2014) Adenosine triphosphate drives head and neck cancer pain through P2X2/3 heterotrimers. *Acta Neuropathol. Commun.* **2,** 62
13. Ford, A. P. (2012) In pursuit of P2X3 antagonists: novel therapeutics for chronic pain and afferent sensitization. *Purinergic Signal.* **8,** 3–26
14. Gunosewoyo, H., and Kassiou, M. (2010) P2X purinergic receptor ligands: recently patented compounds. *Expert Opin. Ther. Pat.* **20,** 625–646
15. Chen, C. C., Akopian, A. N., Sivilotti, L., Colquhoun, D., Burnstock, G., and Wood, J. N. (1995) A P2X purinoceptor expressed by a subset of sensory neurons. *Nature* **377,** 428–431
16. Brass, D., Grably, M. R., Bronstein-Sitton, N., Gohar, O., and Meir, A. (2012) Using antibodies against P2Y and P2X receptors in purinergic signaling research. *Purinergic Signal.* **8,** 61–79
17. Grubb, B. D., and Evans, R. J. (1999) Characterization of cultured dorsal root ganglion neuron P2X receptors. *Eur. J. Neurosci.* **11,** 149–154
18. Gum, R. J., Wakefield, B., and Jarvis, M. F. (2012) P2X receptor antagonists for pain management: examination of binding and physicochemical properties. *Purinergic Signal.* **8,** 41–56
19. Burnstock, G., and Kennedy, C. (2011) P2X receptors in health and disease. *Adv. Pharmacol.* **61,** 333–372
20. Keystone, E. C., Wang, M. M., Layton, M., Hollis, S., McInnes, I. B., and D1520C00001 Study Team (2012) Clinical evaluation of the efficacy of the P2X7 purinergic receptor antagonist AZD9056 on the signs and symptoms of rheumatoid arthritis in patients with active disease despite treatment with methotrexate or sulphasalazine. *Ann. Rheum. Dis.* **71,** 1630–1635
21. Stock, T. C., Bloom, B. J., Wei, N., Ishaq, S., Park, W., Wang, X., Gupta, P., and Mebus, C. A. (2012) Efficacy and safety of CE-224,535, an antagonist

of P2X7 receptor, in treatment of patients with rheumatoid arthritis inadequately controlled by methotrexate. *J. Rheumatol.* **39,** 720–727
22. Baqi, Y., Hausmann, R., Rosefort, C., Rettinger, J., Schmalzing, G., and Müller, C. E. (2011) Discovery of potent competitive antagonists and positive modulators of the P2X2 receptor. *J. Med. Chem.* **54,** 817–830
23. Gever, J. R., Soto, R., Henningsen, R. A., Martin, R. S., Hackos, D. H., Panicker, S., Rubas, W., Oglesby, I. B., Dillon, M. P., Milla, M. E., Burnstock, G., and Ford, A. P. (2010) AF-353, a novel, potent and orally bioavailable P2X3/P2X2/3 receptor antagonist. *Br. J. Pharmacol.* **160,** 1387–1398
24. Ford, A. P., and Undem, B. J. (2013) The therapeutic promise of ATP antagonism at P2X3 receptors in respiratory and urological disorders. *Front. Cell Neurosci.* **7,** 267
25. Abdulqawi, R., Dockry, R., Holt, K., Layton, G., McCarthy, B. G., Ford, A. P., and Smith, J. A. (2015) P2X3 receptor antagonist (AF-219) in refractory chronic cough: a randomized, double-blind, placebo-controlled phase 2 study. *Lancet* **385,** 1198–1205
26. Goswami, S., Wang, W., Arakawa, T., and Ohtake, S. (2013) Developments and challenges for mAb-based therapeutics. *Antibodies* **2,** 452–500
27. Buell, G., Chessell, I. P., Michel, A. D., Collo, G., Salazzo, M., Herren, S., Gretener, D., Grahames, C., Kaur, R., Kosco-Vilbois, M. H., and Humphrey, P. P. (1998) Blockade of human P2X7 receptor function with a monoclonal antibody. *Blood* **92,** 3521–3528
28. Reeves, P. J., Callewaert, N., Contreras, R., Khorana, H. G. (2002) Structure and function in rhodopsin: high-level expression of rhodopsin with restricted and homogeneous *N*-glycosylation by a tetracycline-inducible *N*-acetylglucosaminyltransferase I-negative HEK293S stable mammalian cell line. *Proc. Natl. Acad. Sci. U.S.A.* **99,** 13419–13424
29. Wesselmann, U., Czakanski, P. P., Affaitati, G., and Giamberardino, M. A. (1998) Uterine inflammation as a noxious visceral stimulus: behavioral characterization in the rat. *Neurosci. Lett.* **246,** 73–76
30. Hargreaves, K., Dubner, R., Brown, F., Flores, C., and Joris, J. (1988) A new and sensitive method for measuring thermal nociception in cutaneous hyperalgesia. *Pain* **32,** 77–88
31. Gonzales, E. B., Kawate, T., and Gouaux, E. (2009) Pore architecture and ion sites in acid sensing ion channels and P2X receptors. *Nature* **460,** 599–604
32. Pontén, J., and Macintyre, E. H. (1968) Long term culture of normal and neoplastic human glia. *Acta Pathol. Microbiol. Scand.* **74,** 465–486
33. Wirkner, K., Sperlagh, B., and Illes, P. (2007) P2X3 receptor involvement in pain states. *Mol. Neurobiol.* **36,** 165–183
34. Ueno, S., Tsuda, M., Iwanaga, T., and Inoue, K. (1999) Cell type-specific ATP-activated responses in rat dorsal root ganglion neurons. *Br. J. Pharmacol.* **126,** 429–436
35. Burgard, E. C., Niforatos, W., van Biesen, T., Lynch, K. J., Touma, E., Metzger, R. E., Kowaluk, E. A., and Jarvis, M. F. (1999) P2X receptor-mediated ionic currents in dorsal root ganglion neurons. *J. Neurophysiol.* **82,** 1590–1598
36. Golay, J., and Introna, M. (2012) Mechanism of action of therapeutic monoclonal antibodies: promises and pitfalls of *in vitro* and *in vivo* assays. *Arch. Biochem. Biophys.* **526,** 146–153
37. Garcia-Guzman, M., Stühmer, W., and Soto, F. (1997) Molecular characterization and pharmacological properties of the human P2X3 purinoceptor. *Brain Res. Mol. Brain Res.* **47,** 59–66
38. Collo, G., North, R. A., Kawashima, E., Merlo-Pich, E., Neidhart, S., Surprenant, A., and Buell, G. (1996) Cloning of P2X5 and P2X6 receptors and the distribution and properties of an extended family of ATP-gated ion channels. *J. Neurosci.* **16,** 2495–2507
39. Evans, R. J., and Surprenant, A. (1996) P2X receptors in autonomic and sensory neurons. *Semin. Neurosci.* **8,** 217–223
40. Rae, M. G., Rowan, E. G., and Kennedy, C. (1998) Pharmacological properties of P2X3-receptors present in neurons of the rat dorsal root ganglia. *Br. J. Pharmacol.* **124,** 176–180
41. Petruska, J. C., Mena, N., Nakatsuka, T., Cooper, B. Y., Johnson, R. D., and Gu, J. G. (2000) P2X1 receptor subunit immunoreactivity and ATP-evoked fast currents in adult rat dorsal root ganglion neurons. *Neuroreport* **11,** 3589–3592
42. Kobayashi, K., Fukuoka, T., Yamanaka, H., Dai, Y., Obata, K., Tokunaga, A., and Noguchi, K. (2005) Differential expression patterns of mRNAs for P2X receptor subunits in neurochemically characterized dorsal root ganglion neurons in the rat. *J. Comp. Neurol.* **481,** 377–390
43. De Roo, M., Rodeau, J. L., and Schlichter, R. (2003) Dehydroepiandrosterone potentiates native ionotropic ATP receptors containing the P2X2 subunit in rat sensory neurones. *J. Physiol.* **552,** 59–71
44. De Roo, M., Boué-Grabot, E., and Schlichter, R. (2010) Selective potentiation of homomeric P2X2 ionotropic ATP receptors by a fast non-genomic action of progesterone. *Neuropharmacology* **58,** 569–577
45. Paukert, M., Osteroth, R., Geisler, H. S., Brandle, U., Glowatzki, E., Ruppersberg, J. P., and Gründer, S. (2001) Inflammatory mediators potentiate ATP-gated channels through the $P2X_3$ subunit. *J. Biol. Chem.* **276,** 21077–21082
46. Grishin, E. V., Savchenko, G. A., Vassilevski, A. A., Korolkova, Y. V., Boychuk, Y. A., Viatchenko-Karpinski, V. Y., Nadezhdin, K. D., Arseniev, A. S., Pluzhnikov, K. A., Kulyk, V. B., Voitenko, N. V., and Krishtal, O. O. (2010) Novel peptide from spider venom inhibits P2X3 receptors and inflammatory pain. *Ann. Neurol.* **67,** 680–683
47. Pratt, E. B., Brink, T. S., Bergson, P., Voigt, M. M., and Cook, S. P. (2005) Use-dependent inhibition of P2X3 receptors by nanomolar agonist. *J. Neurosci.* **25,** 7359–7365
48. Robinson, L. E., and Murrell-Lagnado, R. D. (2013) The trafficking and targeting of P2X receptors. *Front. Cell Neurosci.* **7,** 233
49. Vacca, F., Giustizieri, M., Ciotti, M. T., Mercuri, N. B., and Volonté, C. (2009) Rapid constitutive and ligand-activated endocytic trafficking of P2X receptor. *J. Neurochem.* **109,** 1031–1041
50. Chen, X. Q., Zhu, J. X., Wang, Y., Zhang, X., and Bao, L. (2014) CaMKIIα and caveolin-1 cooperate to drive ATP-induced membrane delivery of the P2X3 receptor. *J. Mol. Cell Biol.* **6,** 140–153
51. Fabbretti, E., D'Arco, M., Fabbro, A., Simonetti, M., Nistri, A., and Giniatullin, R. (2006) Delayed upregulation of ATP P2X3 receptors of trigeminal sensory neurons by calcitonin gene-related peptide. *J. Neurosci.* **26,** 6163–6171
52. Jarvis, M. F., Burgard, E. C., McGaraughty, S., Honore, P., Lynch, K., Brennan, T. J., Subieta, A., Van Biesen, T., Cartmell, J., Bianchi, B., Niforatos, W., Kage, K., Yu, H., Mikusa, J., Wismer, C. T., *et al.* (2002) A-317491, a novel potent and selective non-nucleotide antagonist of P2X3 and P2X2/3 receptors, reduces chronic inflammatory and neuropathic pain in the rat. *Proc. Natl. Acad. Sci. U.S.A.* **99,** 17179–17184
53. Lu, S. H., Groat, W. C., Lin, A. T., Chen, K. K., and Chang, L. S. (2007) Evaluation of purinergic mechanism for the treatment of voiding dysfunction: a study in conscious spinal cord-injured rats. *J. Chin. Med. Assoc.* **70,** 439–444
54. Ohashi, K., Kawai, M., Ninomiya, N., Taylor, C., and Kurebayashi, Y. (2008) Effect of a new α 2 δ ligand PD-217014 on visceral hypersensitivity induced by 2,4,6-trinitrobenzene sulfonic acid in rats. *Pharmacology* **81,** 144–150
55. McGaraughty, S., Wismer, C. T., Zhu, C. Z., Mikusa, J., Honore, P., Chu, K. L., Lee, C. H., Faltynek, C. R., and Jarvis, M. F. (2003) Effects of A-317491, a novel and selective P2X3/P2X2/3 receptor antagonist, on neuropathic, inflammatory and chemogenic nociception following intrathecal and intraplantar administration. *Br. J. Pharmacol.* **140,** 1381–1388
56. Shields, S. D., Cavanaugh, D. J., Lee, H., Anderson, D. J., and Basbaum, A. I. (2010) Pain behavior in the formalin test persists after ablation of the great majority of C-fiber nociceptors. *Pain* **151,** 422–429